

Final Technical Report
USGS Award G10AP00077
PI: Jacobo Bielak

**THREE-DIMENSIONAL NONLINEAR EARTHQUAKE GROUND MOTION
SIMULATION IN THE SALT LAKE BASIN USING THE WASATCH FRONT
COMMUNITY VELOCITY MODEL**

Doriam Restrepo, Ricardo Taborda and Jacobo Bielak*

Computational Seismology Laboratory
Department of Civil and Environmental Engineering
Carnegie Mellon University
Pittsburgh, PA 15213-3890

*Corresponding Author
Office: 123H Porter Hall
P: 412-268-2958 F: 412-268-7813
Email: jbielak@cmu.edu

January 9, 2012

ABSTRACT

Forty percent of the population in Utah lives in the Salt Lake Basin, in the vicinity of the Wasatch Front. This front, formed by the Wasatch fault, poses a significant seismic hazard. Recently, there has been an increased effort to understand the levels of excitation and ground response expected in the Salt Lake Basin. The development of the Wasatch Front Community Velocity Model has made it possible for the first time to analyze, through simulations, the relative importance of factors such as the depth of the sedimentary deposits, edge effects, and focusing, that influence ground shaking in this region. Another factor that has been observed to influence strong ground motion is the extent of inelastic deformation that occurs during an earthquake. This report presents results from a set of full three-dimensional (3D) simulations incorporating nonlinear soil behavior in the soft-soil deposits ($V_s \leq 500$ m/s) in the basin, under a Mw 6.8 scenario earthquake. Simulations are performed using Hercules, the finite-element octree-based parallel earthquake simulator developed by the Quake Group at Carnegie Mellon University. Hercules incorporates a rate-dependent approach to simulate the elasto-visco-plastic behavior of soil materials. Our results are qualitatively consistent with observations from past earthquakes. They indicate that nonlinear soil behavior greatly affects the spatial variability of the ground motion, causes permanent displacements, and reduces peak ground velocities and accelerations. They also indicate that nonlinearity is influenced by 3D effects that cannot be reproduced by alternative hybrid or pseudo-nonlinear approaches commonly used in seismic hazard analysis.

THREE-DIMENSIONAL NONLINEAR EARTHQUAKE GROUND MOTION SIMULATION IN THE SALT LAKE BASIN USING THE WASATCH FRONT COMMUNITY VELOCITY MODEL

INTRODUCTION

The Wasatch fault, located along the western edge of the Wasatch Range with the Great Basin in north-central United States, is a normal fault system composed of several sub-faults of about 25 miles each, stretching 240 miles from central Utah to south Idaho. It is the longest fault of its type in the world and one of the most active. Although most of its recent activity has resulted in small magnitude earthquakes, there is geologic evidence which indicates that it has the potential to generate a moderate to large magnitude earthquake greater than 6.8 (Machette et al., 1991, 1992; DuRoss, 2008), with a return period of about 360 years (Wong, 2011). The Wasatch Front, a sequence of cities and towns along the range, houses over 80 percent of Utah's total population, and more than 40 percent resides in the Salt Lake Basin alone, between the Utah basin and the Great Lake, in Salt Lake City (see Fig. 1). Thus, the importance of understanding the seismic hazard and quantifying the seismic risk in the region.

Numerous studies have been devoted to understanding the seismicity and faulting characteristics of the Wasatch Front (e.g., Arabasz, 1980; Machette et al., 1991, 1992; DuRoss, 2008; Wong, 2011). There has been, however, limited work dedicated to estimating the levels of ground motion to be expected during moderate to large magnitude earthquakes in the Salt Lake region. This may be due, in part, to the lack of records of significant magnitude that could be used in classical seismic hazard studies and stochastic and empirical ground motion simulations. The recent development of the Wasatch Front Community Velocity Model (WFCVM) (Magistrale et al., 2006) has made it possible for the first time to conduct physics-based simulations and study the response of the Salt Lake Basin in greater detail. During the past two decades there has been significant progress in the simulation of earthquakes using physics-based numerical methods, mainly using finite differences (FD) and finite elements (FE) (e.g., Frankel, 1992; Olsen et al., 2008; Graves, 2008; Bielak et al., 2010). The great majority of deterministic simulations at scale, however, solve the problem of wave propagation under linear elastic conditions considering only the material losses due to internal friction, and do not consider the influence that the nonlinear behavior of shallow, soft-soil deposits may have on the amplitude and spatial distribution of the ground motion during moderate to large magnitude earthquakes.

Although initially controversial among seismologists and engineers (Beresnev and Wen, 1996), it is now well-accepted that during moderate to large magnitude earthquakes the soil may behave nonlinearly, thus changing considerably the ground motion. Common physical manifestations of this behavior are: reduction in shear wave velocity and increase in the soil internal friction. Other effects are: permanent displacements not associated with the source dislocation, reductions of peak ground velocity and peak ground acceleration (i.e., reductions in amplification with respect to expected linear behavior based on smaller earthquakes), and soil liquefaction (e.g., Darragh and Shakal, 1991; Wen, 1994; Field et al., 1997). The incorporation of nonlinear soil effects has been mostly limited to one- and two-dimensional studies (e.g., Elgamal, 1991; Marsh et al., 1995; Zhang and Papageorgiou, 1996). Such studies have helped corroborate observations and quantify the potential effects. These efforts, however, can only approximately represent three-dimensional (3D) effects. To partially remedy this situation, nonlinear soil behavior has been incorporated into 3D earthquake simulations through hybrid procedures that combine 3D linear with 1D local nonlinear simulations, where the motion obtained at rock sites or in the underlying bedrock is used to solve a nonlinear 1D wave propagation problem under vertically incident waves to obtain the modified response at the surface (e.g., Frankel et al., 2002; Archuleta et al., 2003).

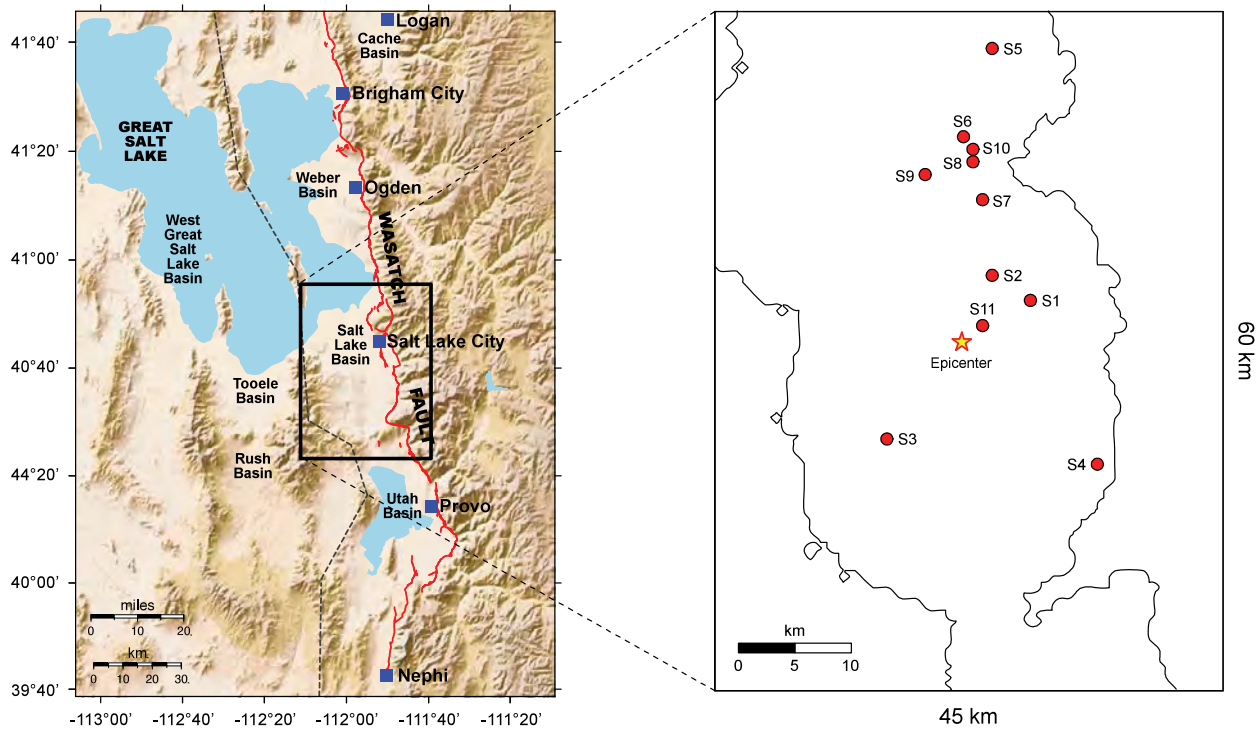


Figure 1. Region of interest, location in the Great Lake Basin and dimensions of the simulation domain and detail of the basin boundary, epicenter, and location of selected stations of interest for later reference.

Due to the computational complexity involved in the incorporation of full 3D nonlinear soil behavior in earthquake simulations, there are only a limited number of nonlinear studies at a regional scale (Xu et al., 2003; Dupros et al., 2010; Taborda, 2010; Taborda and Bielak, 2011). Xu et al. (2003) used a finite element methodology to study the response of an idealized basin ($4 \text{ km} \times 4 \text{ km} \times 1 \text{ km}$) under vertically incident SH waves, considering the soil within the basin as a Drucker-Prager material. Their results showed that peak accelerations decrease due to soil nonlinearity, and that the spatial variation of the surface motion follows that of the linear model, having clear 3D basin effects. They also observed permanent deformations and reductions in peak ground accelerations by factors of about 2 in the deepest regions of the basin, where the shear strains were the largest. Taborda (2010) and Taborda and Bielak (2011) also used FE but implemented an explicit rate-dependent methodology to represent the elasto-visco-plastic behavior of soils. They studied the nonlinear response of the Mygdonian basin in Northern Greece, in a simulation domain of $16 \text{ km} \times 29 \text{ km} \times 41 \text{ km}$. Their results consistently showed reductions of peak velocities and accelerations across the valley by factors ≥ 2 with respect to the linear case, and the presence of significant permanent deformations away from the source. They also noticed increased levels of energy in high frequency and delays in the propagation of waves. These observations are usually regarded as evidence of nonlinear soil behavior in strong motion records. Recently, Dupros et al. (2010) reported on the implementation of an implicit FE scheme and a nonlinear constitutive model to study the effects of inelastic soil behavior in the upper layer of a model of size $30 \text{ km} \times 23 \text{ km} \times 10 \text{ km}$ in the French Riviera. Their results were in agreement with previous studies.

This report builds upon our previous work on the implementation of a rate-dependent approach for modeling nonlinear soil behavior in large-scale 3D physics-based earthquake simulations (Taborda, 2010;

Taborda and Bielak, 2011). It illustrates the effects that soil nonlinearities have on the ground motion in the Salt Lake basin using 3D physics-based simulations at scale. We present a set of simulations under linear and nonlinear soil conditions using Hercules—the octree-based FE parallel earthquake simulator developed by the Quake Group at Carnegie Mellon University (Tu et al., 2006; Taborda et al., 2010). To represent the basin we make use of the WFCVM (Magistrale et al., 2006) for generating a discrete model of the crustal structure and soil deposits in a simulation domain of size 60 km × 45 km × 30 km (Fig. 1). The minimum shear-wave velocity and maximum frequency are taken as 200 m/s and 1 Hz, respectively. The source description corresponds to a scenario earthquake of magnitude Mw 6.8 obtained from an independent dynamic-rupture simulation (Liu and Archuleta, 2011).

NONLINEAR GROUND MOTION MODELING

Earthquake ground motion simulation entails the solution of a wave propagation problem. Under the assumption of small displacements, and linear, isotropic, elastic material, this means solving the semidiscretized version of Navier’s equations of elastodynamics. By applying standard Galerkin ideas with FE in space, we solve for displacements explicitly using central differences in time. Attenuation can be added in the form of viscous damping using different models to introduce the effects of internal friction in the material. In Hercules, this process is done in an element-by-element fashion, which, taking advantage of the unstructured nature of FE meshes, allows one to model efficiently highly heterogeneous systems. Including inelastic soil behavior, however, changes the form in which the internal forces are represented in the semidiscretized version of Navier’s equations, making it necessary to store stresses explicitly, as in

$$M\ddot{u} + C\dot{u} + \sum_e \int_{\Omega_e} B^T \sigma d\Omega_e = f. \quad (1)$$

Here, M and C are the mass and damping matrices, u and f are the displacement and external-force vectors, B is the strain matrix, and σ is the stress tensor over element Ω_e . The summation means assembling of elements. In order to obtain the contribution of internal forces given by the integral term in Equation 1, one must adjust the stresses according to the appropriate material model, yielding rule, and the state of strains. In this research we use the approach described by Taborda (2010) and used in Taborda and Bielak (2011) to introduce soil nonlinearities in large-scale earthquake simulations by means of a rate-dependent methodology, where the contribution due to plastic deformation (\dot{e}^p) is predicted based on the change in the plastic deformation following a power law (Perzyna, 1963) of the form

$$\dot{e}^p = \dot{\lambda} \left\langle \frac{F(\sigma)}{k(\sigma, k)} \right\rangle^{\frac{1}{m}} \frac{\partial g}{\partial \sigma}. \quad (2)$$

CASE STUDY

Material and Numerical Model

The selected region is a model of the crustal structure in the Salt Lake basin in a volume of 60 km × 45 km × 30 km that includes the main urban areas of Salt Lake City, Utah (Fig. 1). The material characteristics in the volume are extracted from the WFCVM developed by Magistrale et al. (2006). The WFCVM incorporates information about the geotechnical and geologic structure of the Wasatch Front. For the near-surface, the WFCVM interpolates the seismic velocities based mainly on isolated direct

measurements (borehole logs) from previous studies (Williams et al., 1993; Schuster and Sun, 1993; Bay et al., 2004). A detailed description of the basic geotechnical units has been given by MacDonald and Ashland (2008). The sub-surface geologic structure of the basin is divided by zones of strong impedance contrast geometrically characterized by three distinct interfaces (Hill, 1990). These three zones are mostly composed of thick sequences of fluvial, lacustrine, and deltaic sediments that reach a maximum thickness of about 3.4 km (see Fig. 2). For the deeper geologic structures in the crust, Moho and upper mantle, the WFCVM uses the results from a collection of studies including local earthquake travel times and standard 1D models for earthquake location.

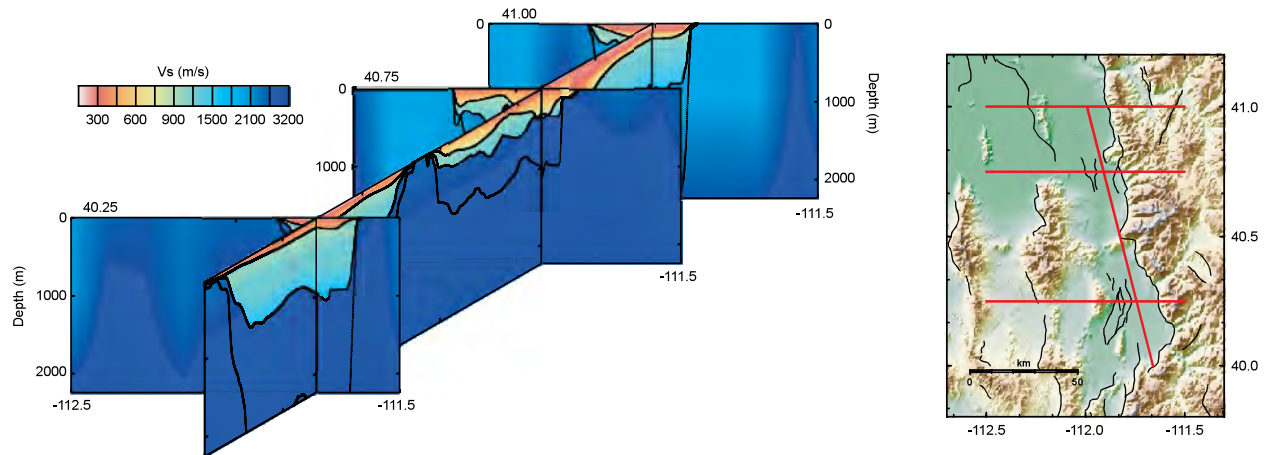


Figure 2. Fence diagram of shear wave velocity along the Wasatch Front in the WFCVM (after Magistrale et al, 2006)..

The simulation domain is represented with an unstructured FE mesh whose elements are tailored to satisfy a minimum shear wave velocity, $V_{s_{\min}} = 200$ m/s and a maximum frequency, $f_{\max} = 1$ Hz. The size of each element (e) is determined based on the rule $e \geq V_s / (p \cdot f_{\max})$, where $p = 8$ is the number of points per wavelength. The resulting mesh has a minimum element size of 25 m and a total of 17.7 million elements. Because of the different stability constraints of the linear and nonlinear runs, the size of the time step (Δt) is also different. For the linear case we used $\Delta t = 0.005$ s, and for the nonlinear case we used $\Delta t = 0.00065$ s. The total simulation time was 75 s. Simulations were run on Kraken, a Cray XT5 system from the U.S. National Institute for Computational Science (NICS). The linear and nonlinear runs took 1.5 hours in 480 cores and 7 hours in 960 cores, respectively.

In the nonlinear simulation we assumed that only the soft-soil deposits were susceptible of plastic deformation. Therefore, only the elements with $V_s \leq 500$ m/s were allowed to behave plastically. All other elements were kept as linear elastic. As a first approximation we only considered nonlinearity in shear deformation and the material was idealized to follow the von Mises yield criterion. Yielding conditions were based on the stress (J_2) histories obtained during a reference linear simulation. On average, the yielding limits used were of about 20 percent the maximum J_2 values registered during the linear simulation. In the future, we plan to use more realistic yielding parameters based on available studies of the soil properties in the region.

Some simplifications were necessary to guarantee the numerical stability of the nonlinear simulation. Due to the fact that the rupture at the fault is represented by an equivalent (kinematic) set of forces at the nodes of the finite elements crossed by the fault plane, such elements and those in its immediate vicinity experience very large (unrealistic) deformations. Far from the fault, the motion generated by these equivalent forces equals that of the prescribed dislocation. Near the fault, however, such large

deformations pose numerical problems for the nonlinear formulation. To avoid this problem we forced the elements in the neighborhood of the fault plane near the surface (depth ≤ 500 m) to remain linear. To this end, we introduced a buffer zone as shown in Fig 3a. This buffer zone follows the orientation of the fault plane and has a thickness of 1 km (500 m in each direction perpendicular to the fault plane). Additional artifacts related to the free-surface condition and the approximation obtained with linear FE also required us to force the elements at the surface to behave linearly at all times. We estimated the impact of these simplifications on the overall response of the valley for a set of simulations with alternate cases where such accommodations were not necessary (e.g., with a source model with a fault plane that does not break to the surface or does not cut through soft-soil elements) and found that such simplifications have a negligible, if at all detectable impact on the response, its amplitude or spatial distribution.

Source Model

The Wasatch fault runs at the base of the mountains that conform the Wasatch range. It displays a normal faulting system composed of ten active segments (Solomon et al., 2004). Measurements of slip and other historical geologic data suggest that some of these segments have the potential to generate earthquakes of magnitude $ML > 6.5$, with a recurrence period of about 250 to 280 years (Cluff et al., 1975, Machette et al., 1991, 1992). For this study we consider an earthquake scenario of magnitude $M_w 6.8$. This scenario was obtained from a dynamic rupture simulation performed by Liu and Archuleta (2010). Both our work and that of Liu and Archuleta are sponsored by the External Research Program of the U.S. Geological Survey, which has fostered during the last few years several research projects oriented to better understand the seismic risk and earthquake hazard in the Salt Lake region. The source model consists of a set of 4646 (46×101) asperities in a fault plane of an area of 28.7×16.6 km². Figure 3a shows the fault plane and the distribution of the final slip. The plane is oriented with a strike and dip of 153° and 50° , respectively. All asperities are normal sub-faults with a rake of 0° . The hypocenter is located at the middle and near the bottom edge of the plane. The rupture propagates upwards, towards the surface, spreads over the fault plane and reaches a maximum slip of about 3 m near the surface. The fault plane has a velocity strengthening zone in a strip of 500 m near the top (surface) edge (Fig. 3a).

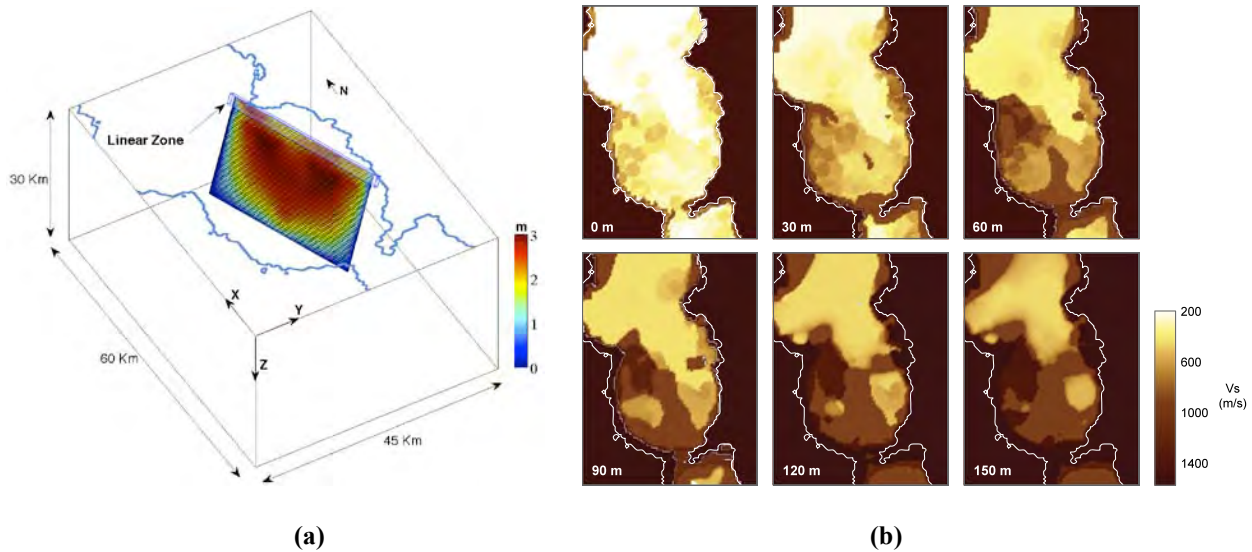


Figure 3. (a) Fault plane location and total slip in the fault. (b) Shear wave velocities of the material model at different depths.

RESULTS

Wave Propagation and Peak Ground Accelerations

We first study the time evolution of the ground motion by comparing the magnitude of the horizontal surface velocities of the nonlinear case with respect to the corresponding linear response, as shown in Fig. 4. We compute the magnitude of peak ground horizontal velocity as the square root of the sum of squares of the NS and EW components of motion at the surface. From Fig. 4 we notice that, as the rupture starts, during the first few seconds of propagation ($t \leq 10$ s), there is little difference between the two cases. This may be due to the motion being primarily controlled by the prescribed source deformation in the neighborhood of the fault plane. Then, as waves travel away from the source ($t \geq 10$ s), the difference in the peak ground velocities becomes more evident. In general, in the areas of greater and clearer contrast within the basin, the nonlinear case exhibits amplitudes of less than half the peak velocities registered under linear conditions. The pattern of propagation in the nonlinear case, however, resembles for the most part that of the linear case. The amplitudes and propagation patterns outside the basin are not changed due to nonlinearities within the basin.

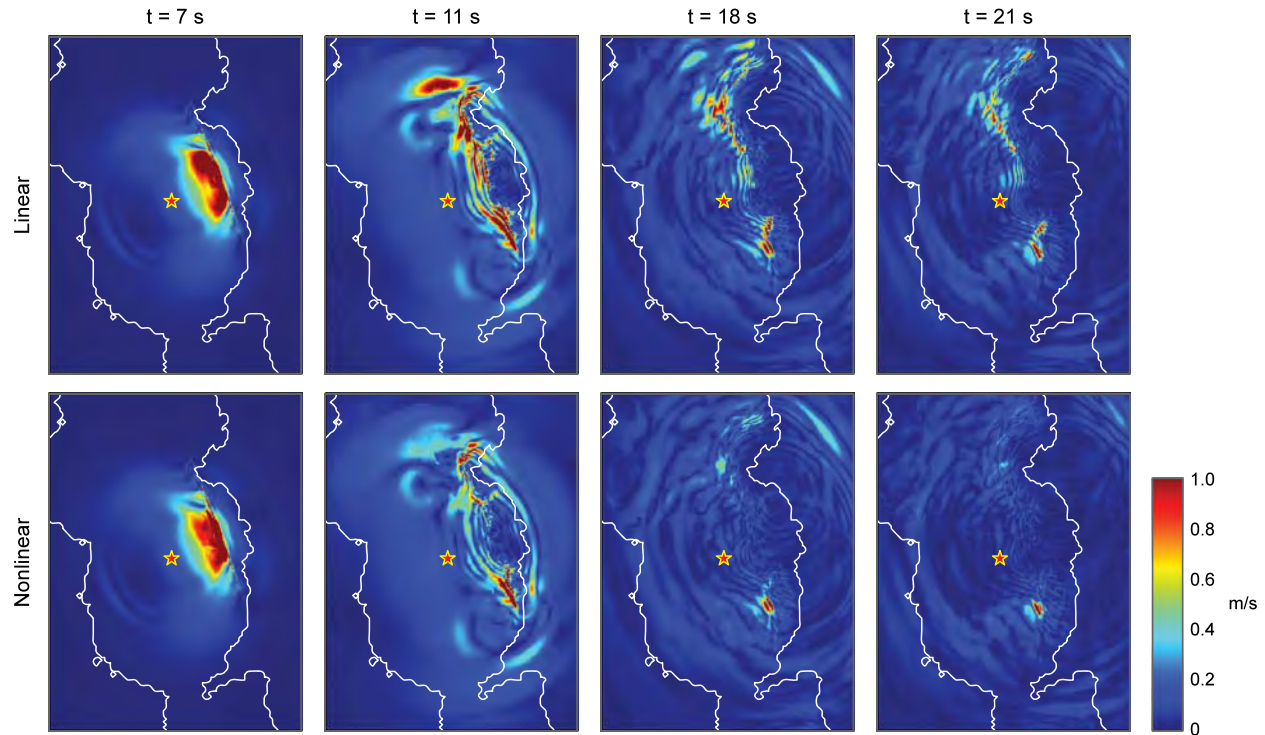


Figure 4. Snapshots of simulations under linear (top) and nonlinear (bottom) soil conditions at different times for the magnitude of the horizontal surface velocity.

From the snapshots at times $t = 11$ and 18 s we observe that the greatest differences are located near the north end of the fault plane where there are sharp contrasts in the spatial distribution of the peak ground response. We associate these differences with the slip distribution of the source model shown in Fig. 3a above, where some of the largest total slips near the surface (in the velocity strengthening fraction of the fault) are concentrated in the upper-north end of the fault. In addition, the localization of greater nonlinear effects in this particular area may also be connected to the shape and soil properties of the basin. Fig. 3b shows that at this location the basin is filled with softer soils than near the south end of the

fault. In addition, it has a natural corner (or rear entry) which can cause greater geometric (edge) effects—especially because of the fault’s proximity to the mountains’ base and the high impedance contrast, which gives rise to complex 3D wave reflections.

These observations can be also summarized by comparing the peak ground horizontal accelerations shown in Fig. 5, for the linear and nonlinear cases. Maxima, in both the linear and nonlinear response concentrate near the fault’s contact with the surface and above the fault plane. By comparing Figs. 5a and 5b, we observe that, in general, the nonlinear case exhibits lower values of peak acceleration than the linear case. The greatest differences are concentrated near the center and north portion of the fault. It is worth mentioning that the color scale in both figures is saturated, i.e., both cases present accelerations larger than 1 g. The nonlinear simulation, however, exhibits smaller areas of saturation than the linear one—showing, again, that the peak accelerations in the nonlinear case are smaller than in the linear one.

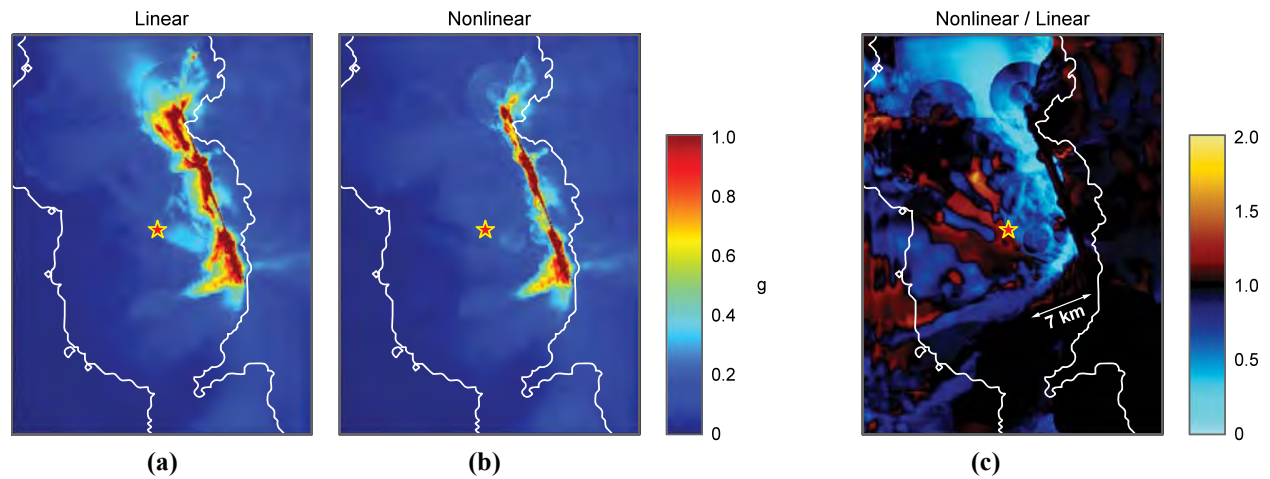


Figure 5. Comparison of the horizontal peak ground surface acceleration for the (a) linear and (b) nonlinear case, as a fraction of gravity; and (c) the ratio between the two cases (nonlinear over linear).

The differences between the linear and nonlinear case are emphasized in Fig. 5c, which shows the ratio of the nonlinear peak response to the linear one. In this figure, warm, red to yellow colors indicate areas where the nonlinear response is larger than that of the linear case. Conversely, cool, blue to cyan colors indicate that the peak ground accelerations in the nonlinear case were smaller than in the linear response. According to evidence from past earthquakes and 1D and 2D nonlinear simulations, the latter ought to be the expected evidence or consequence of nonlinear soil behavior during moderate and strong earthquakes. Fig. 5c suggests that this might not always be the case. We observe that both reductions and amplifications due to nonlinear behavior are present. Near (and above) the fault plane, within a distance of about 7 km, and to the north, reductions due to plastic behavior seem to be the norm—with the peak accelerations of the nonlinear case reaching values as low as 20 to 50 percent those of the linear case. In some areas farther to the west, however, we observe amplifications due to nonlinear behavior, by factors of about 1.2 to 1.5. It is difficult to pinpoint what might have caused these amplifications but it is our initial estimate that they are the result of 3D basin effects—they seem to follow some ray (or bursts) coming from the southern end of the fault plane.

Permanent Displacements

When unrelated to the fault’s dislocation, permanent displacements are regarded as evidence of nonlinear soil behavior. Figures 6a and 6b show the permanent displacement of both the linear and nonlinear

simulations, computed as the average value of displacement over the last 15 seconds of simulation. The two cases present a similar pattern. Maximum permanent displacements are imposed by the slip prescribed at the fault with the largest values at the center near the surface and towards the bottom corners. Both simulations also preserve the same four regions of minima. The nonlinear simulation, however, presents a less homogeneous distribution of the maxima, that is, larger spatial variability of the permanent displacement near the center of the fault plane, and exhibits sharper contrasts in the region of minima near the north end of the fault line.

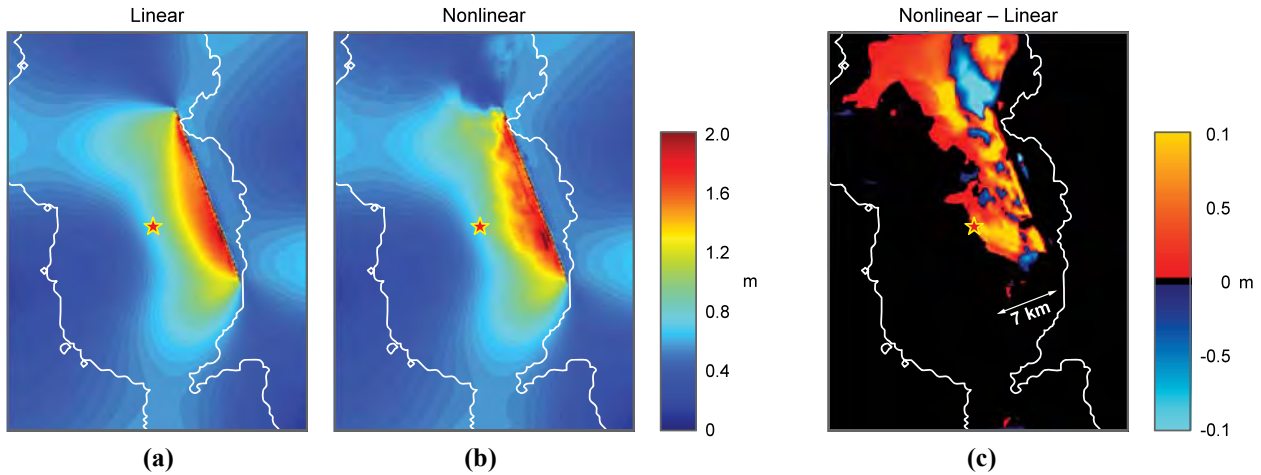


Figure 6. Magnitude of the surface permanent displacements. (a) Linear case, (b) nonlinear case, and (c) nonlinear minus linear.

The discrepancies between the two cases and influence of the plastic deformation in the nonlinear case can be appreciated in greater detail in Fig. 6c. This figure shows the difference in permanent displacements (nonlinear – linear). Warm (red to yellow) colors indicates that the nonlinear permanent displacement was larger than that obtained under elastic soil conditions, and cool (blue to cyan) colors indicate that the permanent displacement observed in the nonlinear simulation was smaller than its counterpart. All the differences are located within the basin and are concentrated near the fault plane and towards the northern area of the simulation domain. This area corresponds closely to the area with the largest reductions in peak ground accelerations (see Fig. 5c), in the deeper portions of the basin’s soft-soil deposits (see Fig. 3b). For the most part, the nonlinear simulation presents larger permanent displacements than the linear one. The smaller regions where this is not the case, especially the area north from the fault line, however, challenge the idea that permanent plastic deformations are always expected to be larger and evidence the presence of complex 3D basin effects. The shallower deposits near and off the south end of the fault plane exhibit almost no difference between the two cases. The relative difference, in all cases, appears to be less than 10 percent.

Local Response

Displacements

We compare now the local response at selected locations throughout the region of interest. Figure 7 shows the displacements in the two horizontal components of motion at five different surface locations (or stations). The location of these stations is indicated in Fig. 1b. All these stations are located in the northern part of the region of interest. Most of them seemed to correspond to areas of significant nonlinear soil effects, which in all cases took place within the first 20 seconds of simulation. Some of them exhibit significant differences in the final permanent deformations between the linear and nonlinear

cases. In the NS direction all stations present similar or larger values of permanent deformation in the nonlinear case than in the linear one—which may be interpreted as the result of a stronger directivity effect. In the EW component of motion, however, there is no consistent pattern. In fact, for the case of station S6, contrary to common belief, the displacements in the nonlinear case are significantly smaller than in the linear case. This indicates the presence of stronger basin effects, possibly related to the proximity to the east boundary of the basin.

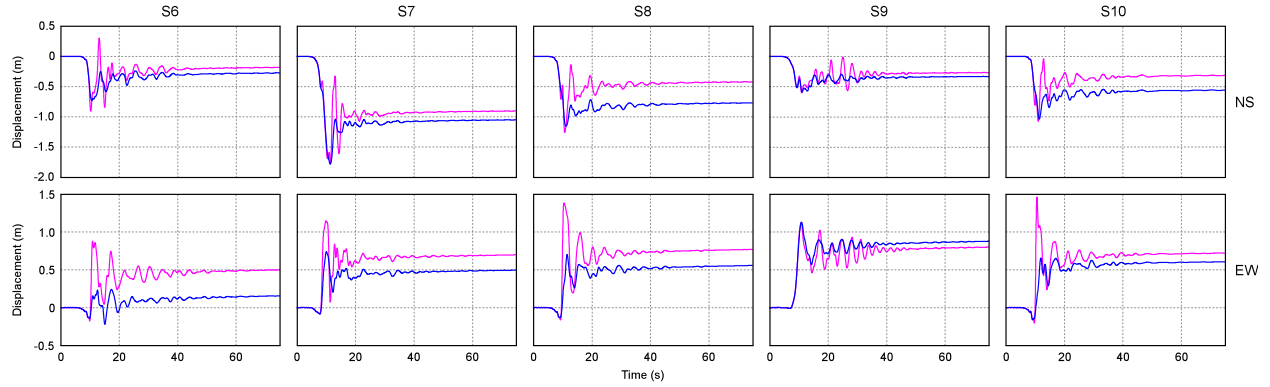


Figure 7. Comparison of the surface linear (magenta) and nonlinear (blue) displacement at stations S6, S7, S8, S9, S10 (see Fig. 1b).

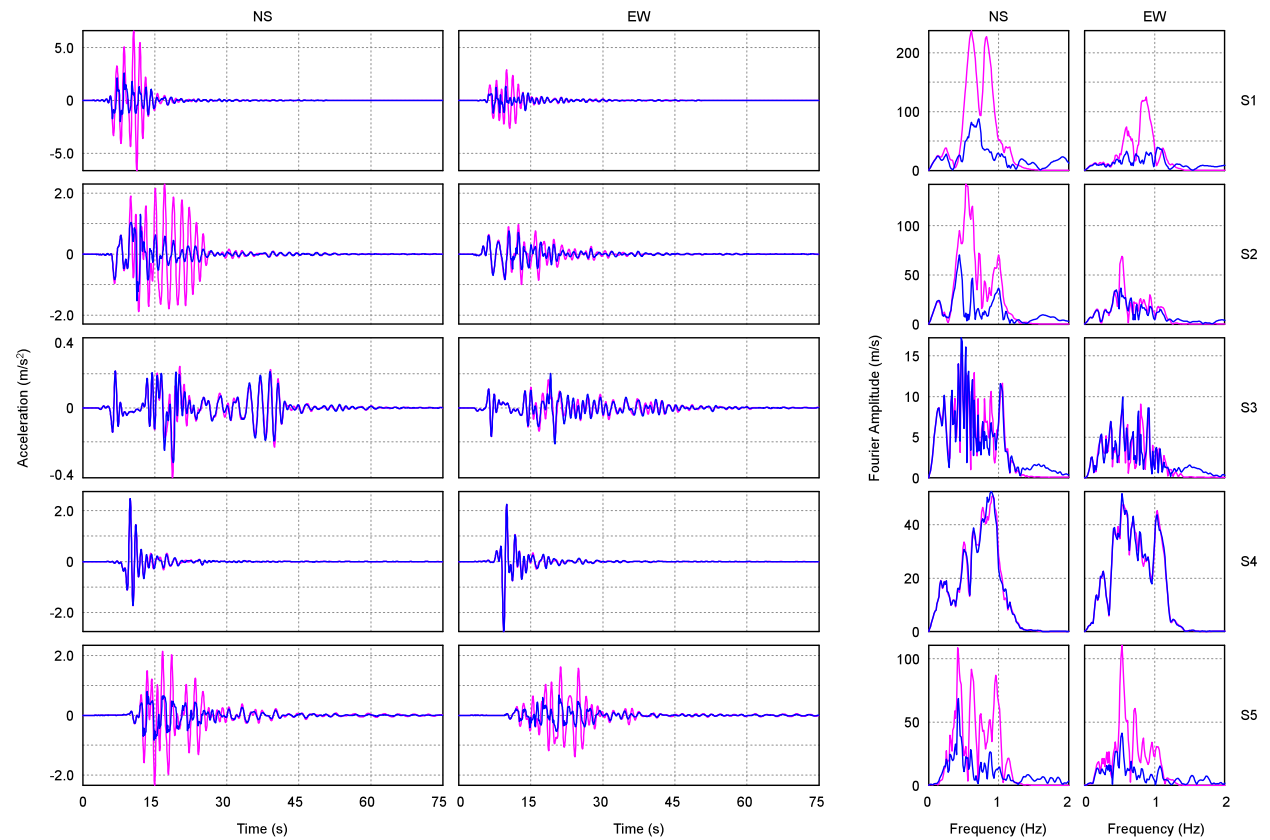


Figure 8. Comparison of the surface linear (magenta) and nonlinear (blue) accelerations (left) and their corresponding Fourier's amplitude spectra (right) in the NS and EW components of motion at stations S1, S2, S3, S4, S5 (see Fig. 1b).

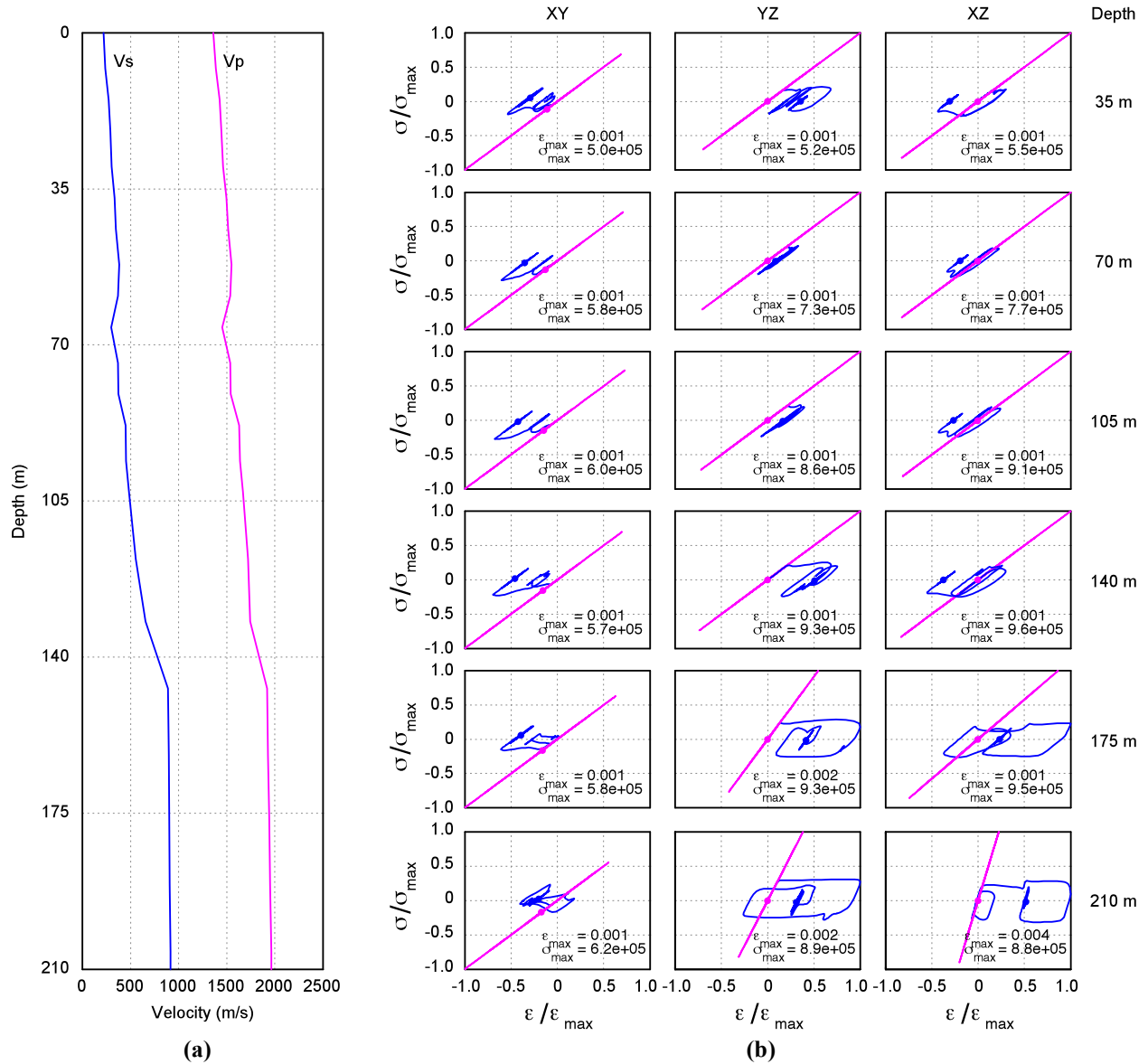


Figure 9. (a) S- (blue) and P- wave (magenta) velocity profiles at station S11. (b) Stress-strain relationships as implicit functions of time at different depths beneath station S11 for the linear (magenta) and nonlinear (blue) simulations, normalized with respect to the absolute maximum values of stress and strain for each case. Solid dots indicate the final state of stresses and deformation.

Accelerations

Figure 8 shows a comparison of the synthetics for ground accelerations at five different stations in both the time and frequency domains for the two horizontal components of motion. The comparison in the time domain confirms the results presented earlier regarding the reductions observed in PGA due to soil nonlinear behavior, especially for those stations near the fault (S1 and S2) and in the northern region of the simulation domain (S5). At these particular locations, the PGA values in the nonlinear case are about 50 percent or smaller than the peak accelerations registered in the linear simulation. For station S2, the reductions are predominant in the NS direction, whereas in S1 and S5 the reductions are of the same order in both components of motion. By contrast, stations S3 and S4 do not show any significant

influence of nonlinearity. Station S4 is near the south end of the fault line and station S3 is farther, southwest from the fault plane. We have already noted that nonlinear soil effects were minimum in these areas due to the shallower deposits, which did not significantly amplify the ground motion, and thus did not develop large levels of excitation beyond the ‘yielding’ limits of the material. The comparisons in the frequency domain consistently show reductions of about 50 percent or more in the amplitude of the nonlinear response with respect to the linear results. Moreover, they indicate that the reductions are mainly in the frequency range between 0.4 and 1.0 Hz (at the maximum simulation frequency). Again, the reductions are predominant in the NS direction. In stations S1 and S2, the changes in the spectra due to plastic behavior in the soil modifies the site’s resonant frequencies. This effect may have important implications in engineering design. Finally, it is noteworthy that the nonlinear case spectra exhibit an increase in the content of energy at frequencies higher than 1 Hz, especially in the NS component of stations S1, S2, and S3. As expected, there is no energy content in the elastic case beyond f_{\max} . In the elastoplastic case, however, the transitions from and to the elastic and plastic states introduce abrupt changes in the response—thus increasing the energy content at frequencies higher than f_{\max} .

Stress-Strain Relationship

Figure 9 shows the shear stress-strain relationships, with time as a parametric variable, for an array of points beneath station S11. The S- and P-wave velocity profiles beneath that station are also shown, down to a depth of 210 m. The more pronounced deformations are present at depths of 175 and 210 m, where strains in the nonlinear case reach values larger than twice the maximum linear strain. In general, shear components xz and yz are dominant over the horizontal xy shear—an expected behavior due to the normal orientation of the fault’s rupture. There is, however, a good amount of coupling between the three components—a 3D effect that cannot be captured with simplified 1D and 2D simulations. In all cases, plastic excursions occur early in the simulation. In xy at all depths and in the three shear components at the shallower observation points, the hysteric behavior is predominantly one-sided with small recoveries.

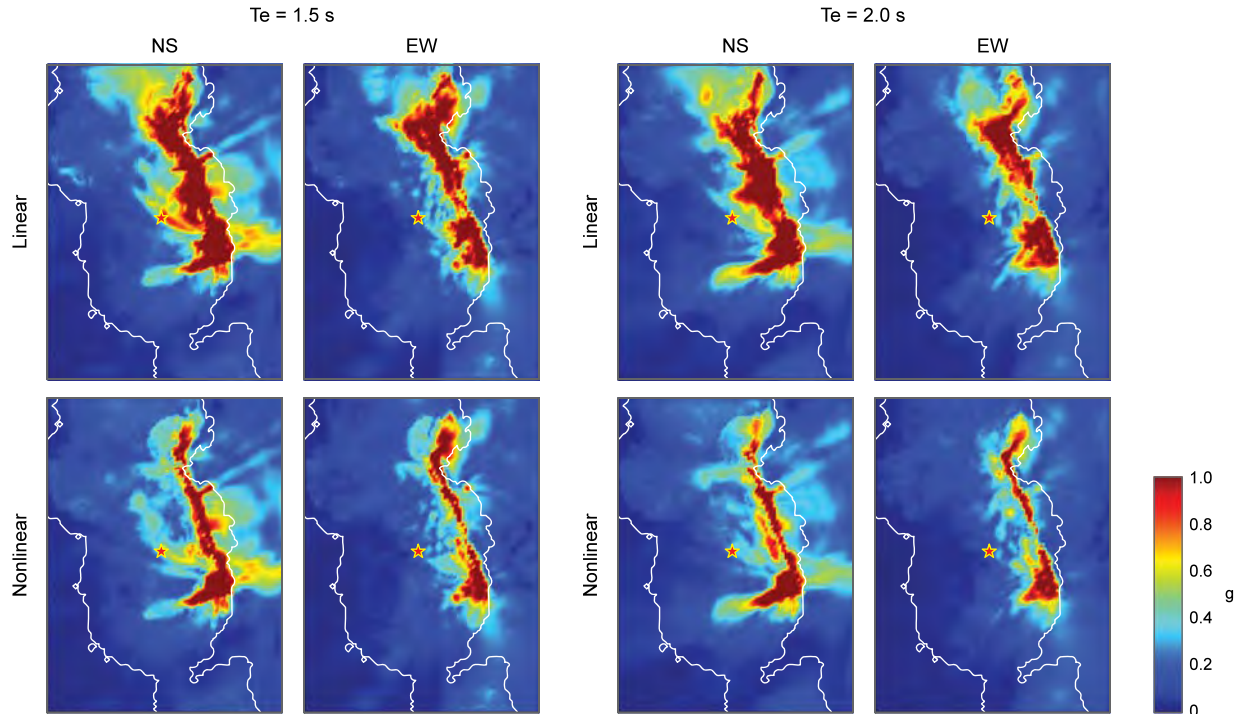


Figure 10. Response spectral acceleration for the linear (top) and nonlinear (bottom) simulations in both the NS and EW components of motion for periods $T_e = 1.5$ and 2.0 s, and critical damping ratio $\zeta = 5\%$.

Implications for Engineering Design

For engineering and structural design purposes, response spectra accelerations continue to be one of the preferred measures of expected seismic demand. Salt Lake City has a mixed urban infrastructure with historical and modern buildings of up to 30-stories high. Knowing the distribution of spectral acceleration (S_a) throughout the valley helps understand the risk certain areas pose for buildings of a particular fundamental period of vibration. Figure 10 shows S_a values throughout the region, obtained from response spectra ordinates for periods $T = 1.5$ and 2.0 s—representative of low- to mid-rise buildings—for 5 percent of critical damping ratio, using the excitations of both the linear and nonlinear simulations. Results for the linear simulation indicate that structures with natural periods in this range and within a distance of about 10 km from the fault line could be exposed to pseudo accelerations larger than 1 g. In the nonlinear case, however, S_a of this level are present only in the immediate vicinity of the fault line (< 2 km) in the central and northern areas. This implies that soil nonlinearities can significantly change the excitation levels—generally a decrease—for particular periods of interest. No changes are observed far from the source or outside the basin.

CONCLUSIONS

We presented an application of a methodology for introducing the effects of nonlinear soil behavior in full 3D deterministic earthquake simulations at regional scales. Results from comparing the ground motion obtained for a MW 6.8 scenario earthquake under linear anelastic and nonlinear elasto-visco-plastic material conditions in the soft-soil deposits in the Salt Lake City basin indicate that soil nonlinearities may cause significant changes in the distribution of permanent deformations, and reductions in peak ground accelerations down to amplitudes of 20 to 50 percent of the peak response obtained under linear anelastic conditions. For the particular case of a normal fault at the edge of the Great Basin with the Wasatch Range, these effects are mainly localized in the vicinity of the fault plane and controlled by the characteristics of the rupture. They underscore the importance that local site effects and soil nonlinearity may have on the ground response, and most importantly, the implications for structural engineering design and analysis. Furthermore, our results confirm that as it is the case in many other applications in ground motion simulation, soil nonlinearities may be influenced by three-dimensional effects that cannot be accurately captured with simplified or approximated solutions. Additional work is still required to properly use and model more realistic properties and characteristics of the soil.

ACKNOWLEDGEMENTS

Research supported by the U.S. Geological Survey (USGS), Department of the Interior, under USGS award number G10AP00077. The views and conclusions contained in this document are those of the authors and should not be interpreted as necessarily representing the official policies, either expressed or implied, of the U.S. Government. We thank Ralph Archuleta and Qiming Liu for providing the seismic source used. This work was also possible thanks to a TeraGrid allocation; computations were performed on Kraken at the National Institute for Computational Sciences.

REFERENCES

- Adachi, T. and F. Oka [1982], “Constitutive equations for normally consolidated clay based on elasto-viscoplasticity”, *Soils and Foundations.*, Vol. 22, No. 4, pp. 57–70.
- Arabasz, W. J., R. B. Smith, and W. D. Richins [1980], “Earthquake studies along the Wasatch front,

- Utah: Network monitoring, seismicity, and seismic hazards”, *Bull. Seism. Soc. Am.*, Vol. 70, No. 5, pp. 1479–1499
- Archuleta, R. J., P. Liu, J. H. Steidl, L. F. Bonilla, D. Lavallée, and F. E. Heuze [2003], “Finite- fault site-specific acceleration time histories that include nonlinear soil response”, *Physics of the Earth and Planetary Interiors*, Vol. 137, pp. 153–181.
- Bay, J., J. Gilbert, F. X. Ashland, G. McDonald, and K. L. Pankow [2004], “2003 SASW shallow shear-wave velocity results”, talk presented at Earthquake Hazards in Utah: Improving Our Understanding, February 26, 2004, Salt Lake City, Utah.
- Beresnev, I. A., and K. L. Wen [1996], “Nonlinear Soil Response-A Reality?”, *Bull. Seism. Soc. Am.*, Vol. 86, No. 6, pp. 1964–1978.
- Bielak, J., R. W. Graves, K. B. Olsen, R. Taborda, L. Ramírez-Guzmán, S. M. Day, G. P. Ely, D. Roten, T. H. Jordan, P. J. Maechling, J. Urbanic, Y. Cui, and G. Juve [2010] “The ShakeOut earthquake scenario: Verification of three simulation sets,” *Geophysical Journal International*, Vol. 180, No. 1, pp. 375–404.
- Cluff, L. S., L. F. Hintze, G. E. Brogan, and C. E. Glass [1975]. “Recent activity of the Wasatch fault, northwestern Utah, USA”, *Tectonophysics* Vol. 29, pp. 161–168.
- Darragh, R. B. and A. F. Shakal [1991], “The site response of two rock and soil station pairs to strong and weak ground motion”, *Bull. Seism. Soc. Am.*, Vol. 81, No. 5, pp. 1885–1899.
- Dupros, F., F. De Martin, E. Foerster, D. Komatitsch, and J. Roman [2010], “High-performance finite-element simulations of seismic wave propagation in three-dimensional nonlinear inelastic geological media”, *Parallel Computing*, Vol. 36, No. 5–6, pp. 308–325.
- DuRoss, C.B. [2008], “Holocene vertical displacement on the central segments of the Wasatch fault zone, Utah”, *Bull. Seism. Soc. Am.*, Vol. 98, pp. 2918–2933.
- Elgamal, A. W. [1991], “Shear hysteretic elasto-plastic earthquake response of soil systems”, *Earthquake Engineering and Structural Dynamics*, Vol. 20, No. 4, pp. 371–387.
- Field, E. H., P. A. Johnson, I. A. Beresnev and Y. Zeng [1997], “Nonlinear ground-motion amplification by sediments during the 1994 Northridge earthquake”, *Nature* Vol. 390, No. 6660, pp. 599–602.
- Frankel, A. and J. Vidale [1992] “A three-dimensional simulation of seismic waves in the Santa Clara Valley, California, from a Loma Prieta aftershock””, *Bull. Seism. Soc. Am.*, Vol. 82, No. 5, pp. 2045–2074.
- Frankel, A. D., and D. L. Carver, R. A. Williams [2002], “Nonlinear and Linear Site Response and Basin Effects in Seattle for the M 6.8 Nisqually, Washington, Earthquake”, *Bull. Seism. Soc. Am.*, Vol. 92, No. 6, pp. 2090–2109.
- Graves, R.W. [2008], “The seismic response of the San Bernardino basin region during the 2001 Big Bear lake earthquake”, *Bull. Seism. Soc. Am.*, Vol. 98, No. 1, pp. 241–252.
- Hill, J., H. Benz., M. Murphy., and G. Schuster [1990], “Propagation and resonance of SH waves in the salt lake valley, Utah”, *Bull. Seism. Soc. Am.*, Vol. 80, No. 1, pp. 23–42.
- Katona, M. G. [1984], “Evaluation of viscoplastic cap model”. *Journal of Geotechnical Engineering.*, ASCE, Vol. 110, No. 8, pp. 1106–1125.
- Liu, Q. and R. Archuleta [2011], Personal communication.
- Machette, M.N., S. F. Personius, A. R. Nelson, D. P. Schwartz, and W. R.. Lund [1991], “The Wasatch fault zone, Utah-segmentation and history of Holocene earthquakes”, *Journal of Structural Geology.*, Vol.13, pp.137–149.

- Machette, M.N., S. F. Personius, and A. R. Nelson [1992], “Paleoseismology of the Wasatch fault zone: A summary of recent investigations, conclusions and interpretations, Chapter A”, in Assessment of Regional Earthquake Hazards and Risk Along the Wasatch Front Area, Utah, U.S. Geological Survey Professional Paper 1500, pp. A1–A71.
- Magistrale, H., K. B. Olsen, and J. C. Pechmann [2006], “Construction and verification of a Wasatch Front Community Velocity Model: Collaborative research with San Diego State University and the University of Utah. Final Technical Report 06HQGR0012, USGS” <http://earthquake.usgs.gov/research/external/reports/06HQGR0012.pdf>.
- Marsh, J., T. J. Larkin, A. J. Haines, and R. A. Benites, R. A. [1995], ”Comparison of linear and nonlinear seismic responses of two-dimensional alluvial basins”, Bull Seism. Soc. Am., Vol. 85, No. 3, pp. 874–889.
- McDonald, G. N., and F. X. Ashland [2008], “Earthquake site conditions in the Wasatch Front urban corridor, Utah”. Special study 125, Utah Geological Survey.
- Olsen, K.B., S.M. Day, J.B. Minster, Y. Cui, A. Chourasia, D. Okaya, P. Maechling and T. Jordan, [2008], “TeraShake2: Spontaneous rupture simulations of MW 7.7 earthquakes on the southern San Andreas fault”, Bull. Seism. Soc. Am., Vol. 98, No. 3, pp. 1162–1185.
- Perzyna, P. [1963], “The constitutive equations for rate sensitive plastic materials,” Quart. of App. Math., Vol. 20, pp. 321–332.
- Schuster, G. T., and Y. Sun [1993], ”Surface wave inversion of near surface shear velocities in Salt Lake Valley”, U.S. Geological Survey Technical Report 1434-92-G-2175, 169 p.
- Solomon, B. J., N. Storey, I. Wong, W. Silva, N. Gregor, D. Wright, and G. McDonald [2004], “Earthquake-hazards scenario for a M7 earthquake on the Salt Lake City segment of the Wasatch fault-zone, Utah”, Special study 111. Utah Geological Survey.
- Taborda. R [2010], “Three dimensional nonlinear soil and site-city effects in urban regions,” Ph.D. dissertation, Civil and Environmental Engineering, Carnegie Institute of Technology, Carnegie Mellon University, Pittsburgh, PA.
- Taborda R. and J. Bielak [2011], “Large-scale earthquake simulation — Computational seismology and complex engineering systems”, Computing in Science and Engineering, Vol. 13, No. 4, pp. 14–26.
- Taborda. R, J. López, H. Karaoglu, J. Urbanic, and J. Bielak [2010], “Speeding up finite element wave propagation for large-scale earthquake simulations”, Technical Report CMU-PDL-10-109, Parallel Data Lab, Carnegie Mellon University.
- Tu, T., H. Yu, L. Ramírez-Guzmán, J. Bielak, O. Ghattas, K-L. Ma, and D. R. O’Hallaron [2006], “From mesh generation to scientific visualization: An end-to-end approach to parallel supercomputing”. In SC ’06: Proceedings of the 2006 ACM/IEEE International Conference for High Performance Computing, Networking, Storage and Analysis, page 15, Tampa, Florida. IEEE Computer Society.
- Wen, K. L. [1994]. “Non-linear soil response in ground motions”, Earthquake Engineering and Structural Dynamics, Vol. 23, No. 6, pp. 599–608.
- Williams, R. A., K. W. King, and J. C. Tinsley [1993], “Site response estimates in Slat Lake Valley, Utah, from borehole seismic velocities”, Bull. Seism. Soc. Am., Vol. 83, No. 3, pp. 862–889.
- Wong, I. G., W. J. Silva, J. Pechmann, R. Darragh, and T. Yu [2011], “Analyses of earthquake source, path, and site factors from ANSS data along Wasatch front, Utah” U.S. Geological Survey Under the National Earthquake Hazards Reduction Program Program Element III Research on Earthquake Occurrence, Physics, and Effects.
- Xu, J., J. Bielak, O. Ghattas, and J. Wang [2003], “Three-dimensional nonlinear seismic ground motion

modeling in basins”. *Physics of The Earth and Planetary Interiors*, 137(1-4), pp. 81–95.

Zhang, B. and A. S. Papageorgiou [1996], “Simulation of the response of the Marina District Basin, San Francisco, California, to the 1989 Loma Prieta earthquake”, *Bull. Seism. Soc. Am.*, Vol. 86, No. 5, pp. 1382–1400.

Zienkiewicz, O. C. and I. C. Corneau [1974], “Visco-plasticity—Plasticity and creep in elastic solids—A unified numerical solution approach”. *International Journal for Numerical Methods in Engineering*, Vol 8, No 4, pp. 821–845.

BIBLIOGRAPHY
(Publications Resulted from this Grant)

This report is a reproduction of the paper presented at the 4th IASPEI / IAEE International Symposium: Effects of Surface Geology on Seismic Motion, held at the University of California, Santa Barbara, August 23–26, 2011. Next is the companion poster presentation. The complete reference of the publication is:

Restrepo D., Taborda R. and Bielak J. (2011). Effects of Soil Nonlinearity on Ground Response in 3D Simulations — An Application to the Salt Lake City Basin. 4th IASPEI / IAEE International Symposium: Effects of Surface Geology on Seismic Motion, University of California, Santa Barbara, August 23–26, 2011.

Effects of Soil Nonlinearity on ground response in 3D Simulations

An application to the Salt Lake City Basin

The Quake Group
at Carnegie Mellon University

Research sponsored by:



Doriam Restrepo, Ricardo Taborda, Jacobo Bielak

Computational Seismology Laboratory
Department of Civil and Environmental Engineering
Carnegie Mellon University

Abstract

Forty percent of the population in Utah lives in the Salt Lake Basin in the vicinity of the Wasatch Front. This front, formed by the Wasatch fault, poses a significant seismic hazard. Recently, there has been an increased effort to understand the levels of excitation and ground response than can be expected in the Salt Lake Basin. The development of the Wasatch Front Community Velocity Model has made it possible for the first time to analyze, through simulations, the relative importance of factors such as the depth of the sedimentary deposits, edge effects, and focusing, that influence ground shaking in this region. Another factor that has been observed to influence strong ground motion is the extent of inelastic deformation that occurs during an earthquake. We present initial results from a set of full three-dimensional (3D) simulations that incorporate nonlinear soil behavior in

the soft-soil deposits ($V_s \leq 500$ m/s) in the basin, under a M_w 6.8 scenario earthquake. Simulations are performed using Hercules, the finite-element octree-based parallel earthquake simulator developed by the Quake Group at Carnegie Mellon University. Hercules incorporates a rate-dependent approach to simulate the elasto-visco-plastic behavior of soil materials. Our results are qualitatively consistent with observations from past earthquakes. They indicate that nonlinear soil behavior greatly affects the spatial variability of the ground motion, causes permanent displacements, and reduces peak ground velocities and accelerations by a factor of about one half. They also indicate that nonlinearity is influenced by 3D effects that cannot be reproduced by alternative hybrid or pseudo-nonlinear approaches commonly used in seismic hazard analysis.

Modeling Inelastic Wave Propagation

We start from the linear momentum equation, shown in (1), in indicial notation. σ_{ij} is the Cauchy tensor of stresses, and f_i and u_i are the body forces and displacements in the i direction. Applying finite elements in space using the standard Galerkin method, preserving the stresses explicitly, and considering the internal friction in the material, we obtain the system of ordinary differential equations shown in (2). M and C are the global mass and damping matrices of the system, and f is the assembled vector of nodal forces. The integral term in (2) represents the internal resistance force, which includes the effect of plastic deformation ($\dot{\epsilon}^p$) that, applying Hooke's law of elasticity, gives σ_{ij} as in (3). The sum over ϵ represents assembly of the finite elements within the domain. B is the strain matrix. For simplicity, we have omitted terms associated with boundary conditions.

$$\sigma_{ij} = E_{ijkl}(\epsilon_{kl} - \epsilon_{kl}^p) \quad (3)$$

$$\dot{\epsilon}_{ij}^p = \lambda_{ij} \left(\frac{F(\sigma_{ij})}{k(\sigma_{ij}, k_{ij})} \right)^{\frac{1}{2}} \frac{\partial g}{\partial \sigma_{ij}} \quad (4)$$

In most geotechnical applications that consider full elastoplastic behavior, the soil is assumed to be rate independent, and $\dot{\epsilon}_{ij}^p$ is often computed through computationally-intensive iterative procedures. By contrast, we have implemented a rate-dependent formulation in which the material strain rate and sensitivity are assumed to be known, and the change in the plastic strain ($\dot{\epsilon}^p$) can be expressed explicitly as a function of the current state of stresses—computed based on a particular constitutive model and material properties—using a flow (power) law of the form proposed by Perzyna (1966), as in (4).

Then, using central differences to express the time derivatives of displacement in (2), and lumping M , we determine the displacement field, u_{n+1} at the next time step (Taborda, 2010).

$$\sigma_{ij,j} + f_i = \rho \ddot{u}_i \quad (1)$$

$$M \ddot{u} + C \dot{u} + \sum_{\epsilon} \int_{\Omega_{\epsilon}} B^T \sigma d\Omega_{\epsilon} = f \quad (2)$$

Case Study: Salt Lake City Basin

The selected region is a model of the crustal structure of the Salt Lake basin. The simulation domain is a volume of 60 km \times 40 km \times 30 km that includes the main urban areas of Salt Lake City, Utah (Fig. 1). We use the Wasatch Front Community Velocity Model (WFCVM) developed by Magistrale *et al.* (2006) to characterize the (elastic) material properties of the domain (Figs 2 and 3). The WFCVM incorporates information about the geotechnical and geologic structure of the Wasatch Front.

The simulation domain is represented with an unstructured finite element mesh of cubes whose elements are tailored to satisfy the local shear wave velocity, down to a minimum of $V_s = 200$ m/s and a maximum frequency, $f_{max} = 1$ Hz. The size of each element (ϵ) is determined based on the rule

$\epsilon \geq V_s / (p f_{max})$, where $p = 8$ is the number of points per wavelength. The resulting mesh has a minimum element size of 25 m and a total of 17.7 million elements. For the simulation considering the nonlinear behavior of soil deposits in the basin, only the finite elements with an elastic $V_s \leq 500$ m/s were allowed to deform visco-plastically. All other elements were kept elastic. In addition, because of the very large strain values imposed in the finite elements located on the fault plane and its immediate vicinity, we introduced a buffer zone within which the material remains anelastic. This buffer zone follows the orientation of the fault plane and has a thickness of 1 km, 500 m in each direction perpendicular to the fault plane (Fig. 4). Free-surface elements were also forced to remain linear to avoid numerical artifacts.

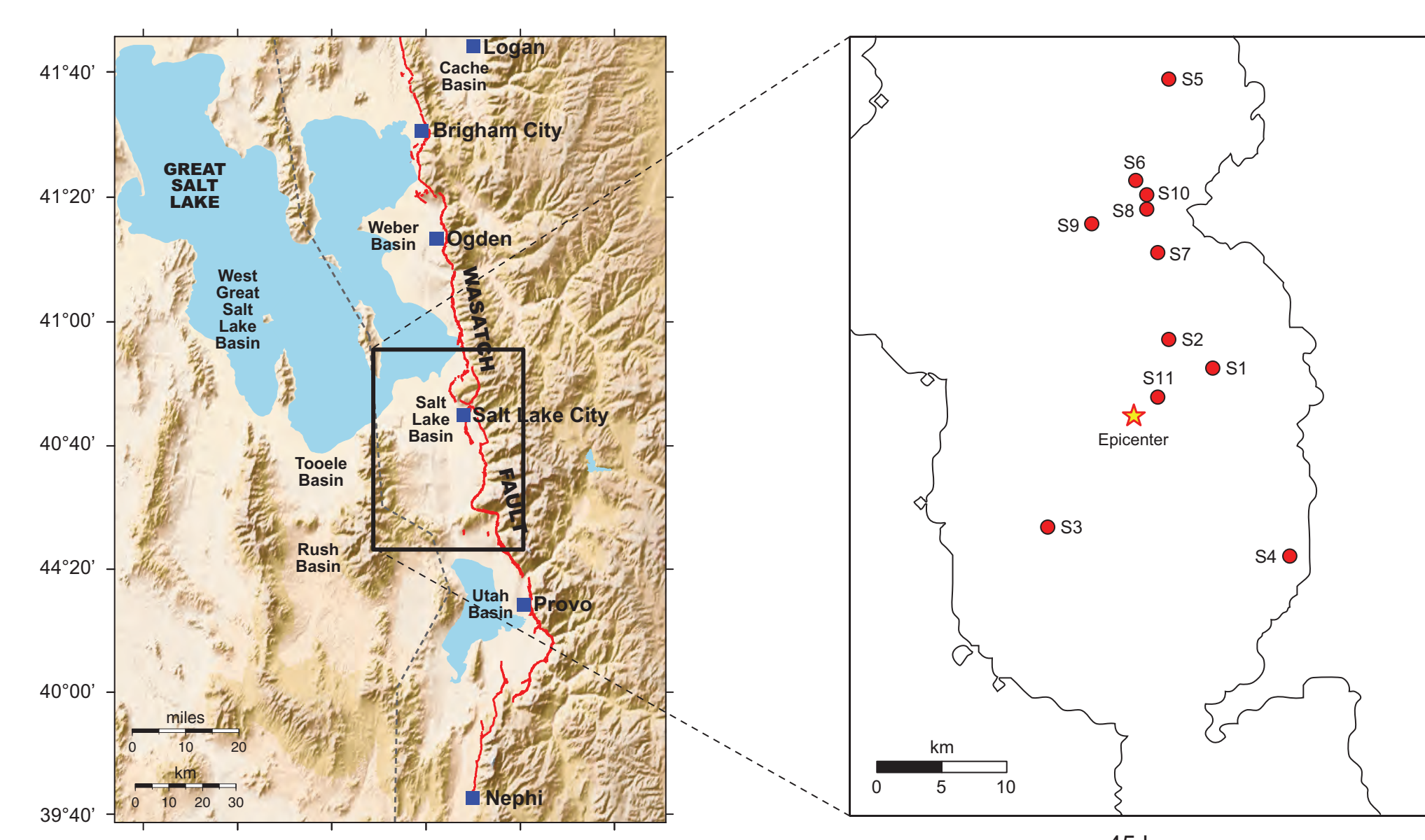


Figure 1: Region of interest and view of the simulation domain.

The fault rupture was obtained from an independent study (Liu and Archuleta, 2011). It corresponds to a M_w 6.8 scenario earthquake. Maximum slip distribution in the fault plane is shown in Fig. 4. For the linear case we used $\Delta t = 0.005$ s, and for the nonlinear case we used $\Delta t = 0.00065$ s.

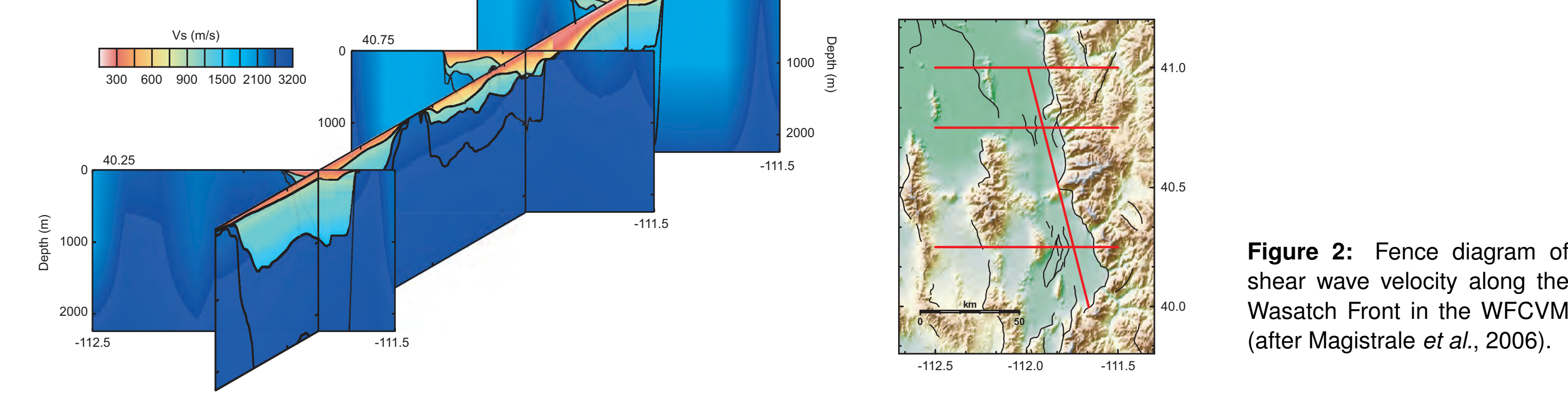


Figure 2: Fence diagram of shear wave velocity along the Wasatch Front in the WFCVM (after Magistrale *et al.*, 2006).

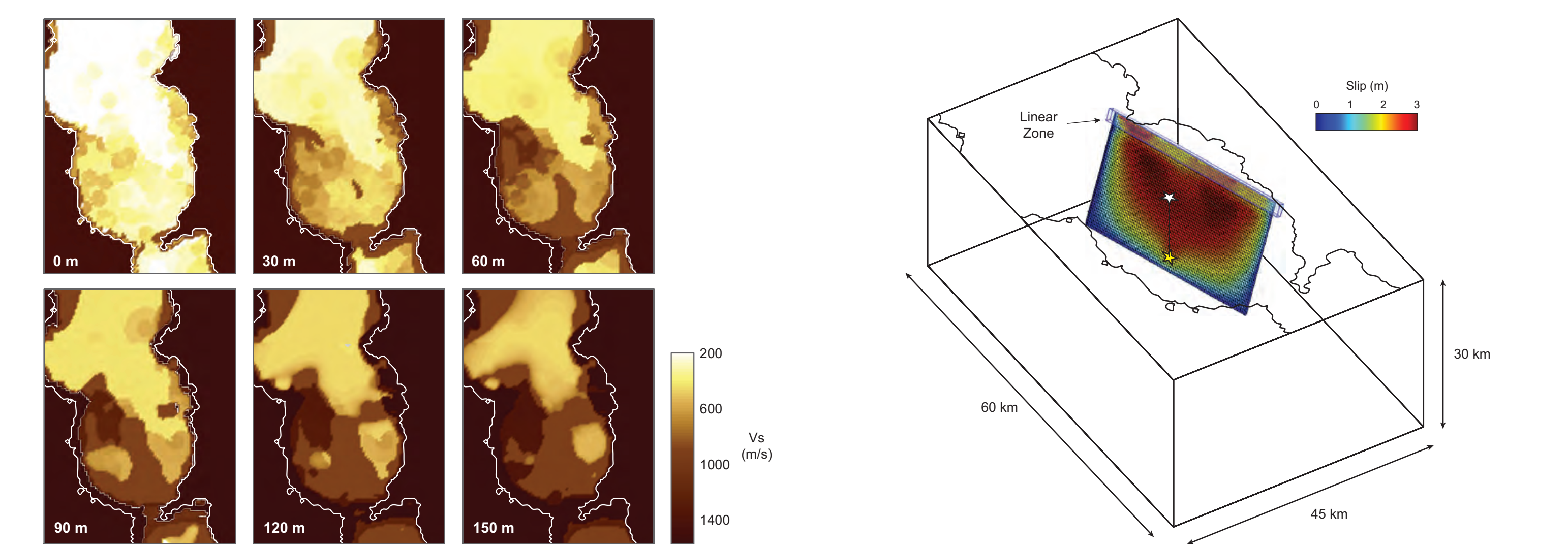


Figure 3: Shear wave velocities of the material model at different depths.

The total simulation time was 75 s. Simulations were run on Kraken, a Cray XT5 system from the U.S. National Institute for Computational Science (NICS). The linear and nonlinear runs took 1.5 hours in 480 cores and 7 hours in 960 cores, respectively.

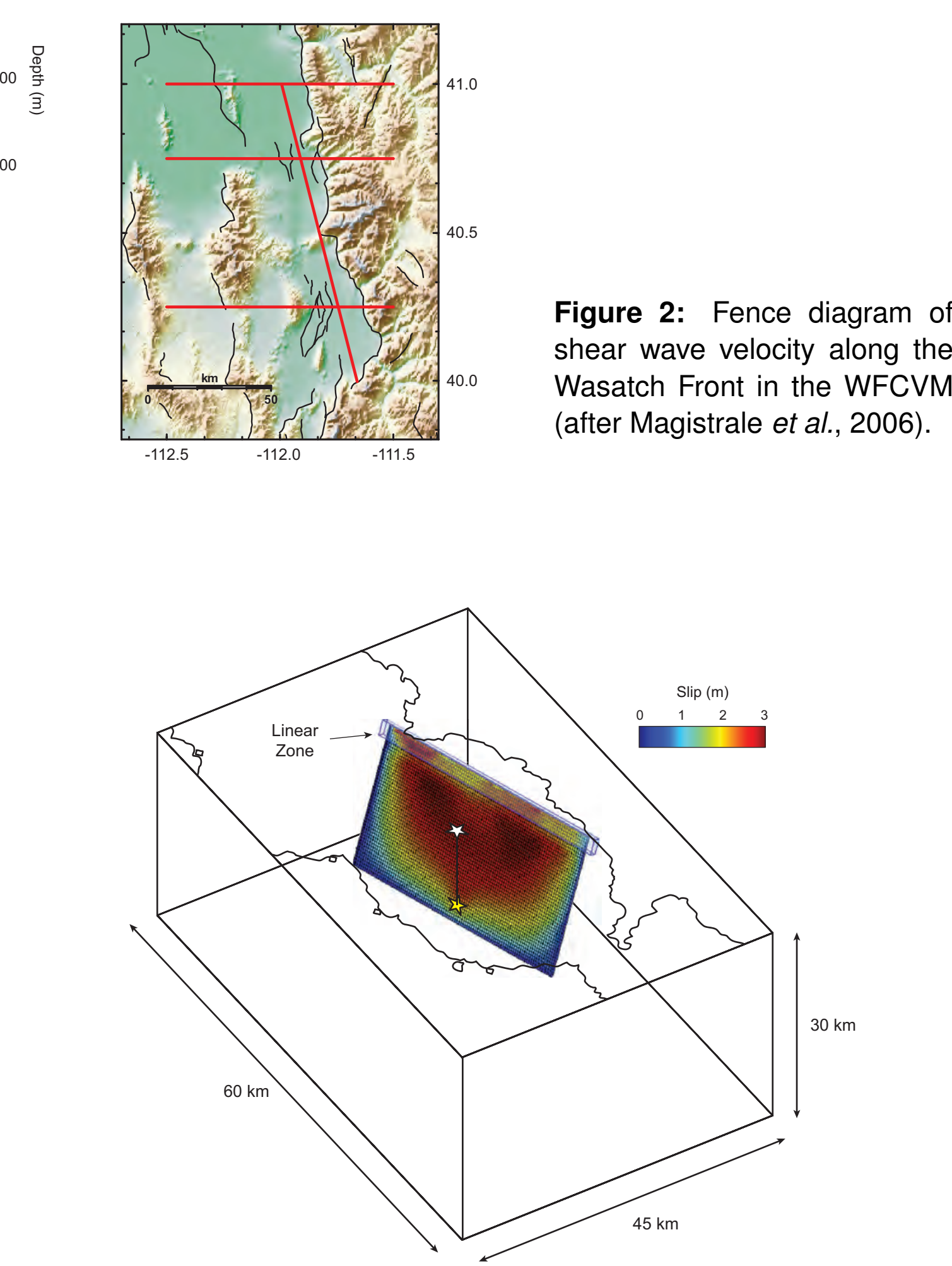


Figure 4: Fault plane location and total slip in the fault.

Results and Analysis

Global Response

Figure 5 shows the magnitude of peak ground horizontal velocity as the square root of the sum of squares of the *NS* and *EW* components of motion at the free surface. From the figures we notice that during the first few seconds of propagation ($t \leq 10$ s), there is little difference between the linear and nonlinear cases. Then, as waves travel away from the source ($t \geq 10$ s), the differences become more evident. In general, in the areas of greater and clearer contrast within the basin, the nonlinear case exhibits amplitudes less than half of the peak velocities registered under linear conditions.

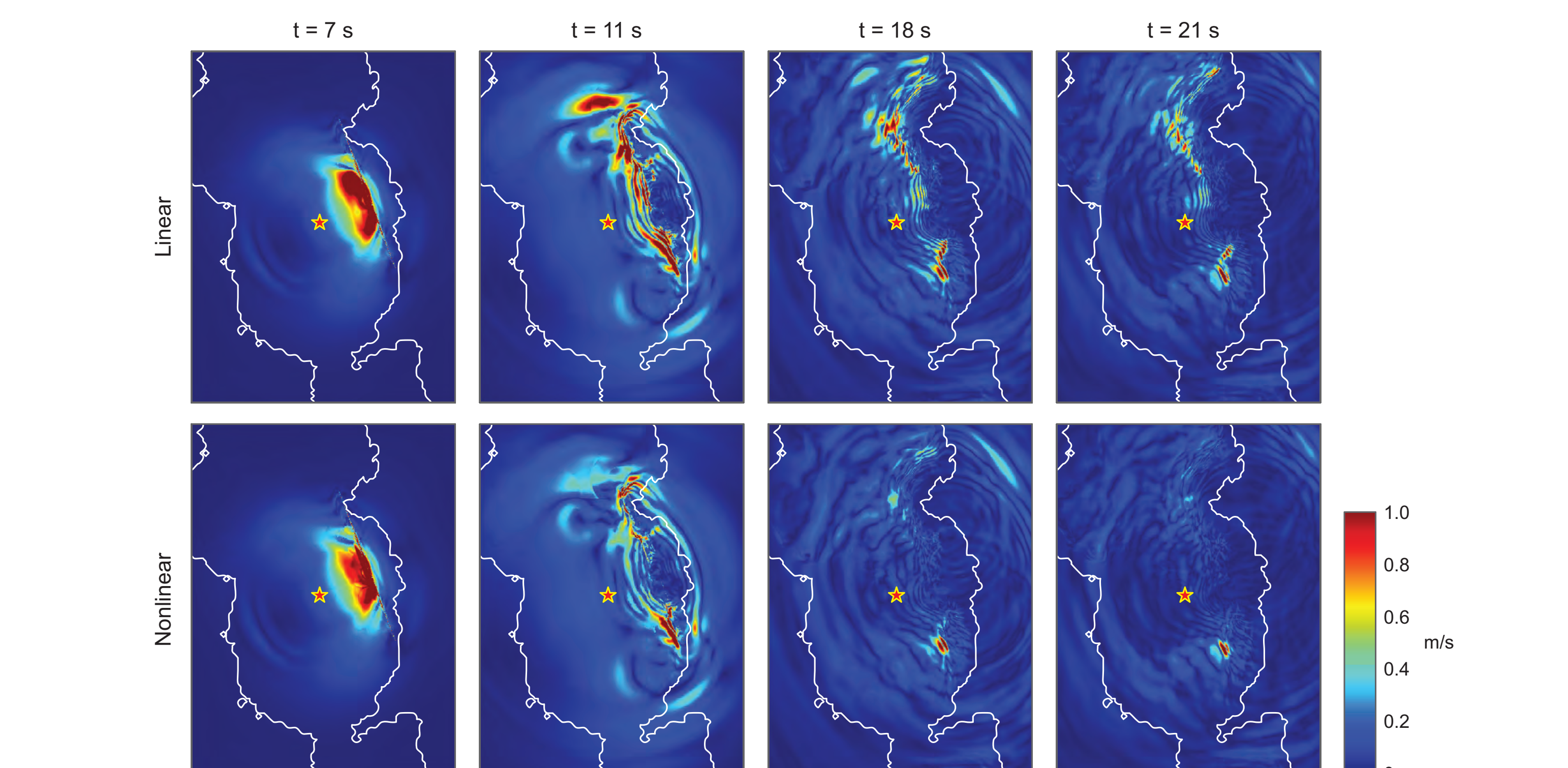


Figure 5: Snapshots of simulations under linear (top) and nonlinear (bottom) soil conditions at different times for the magnitude of the horizontal surface velocity.

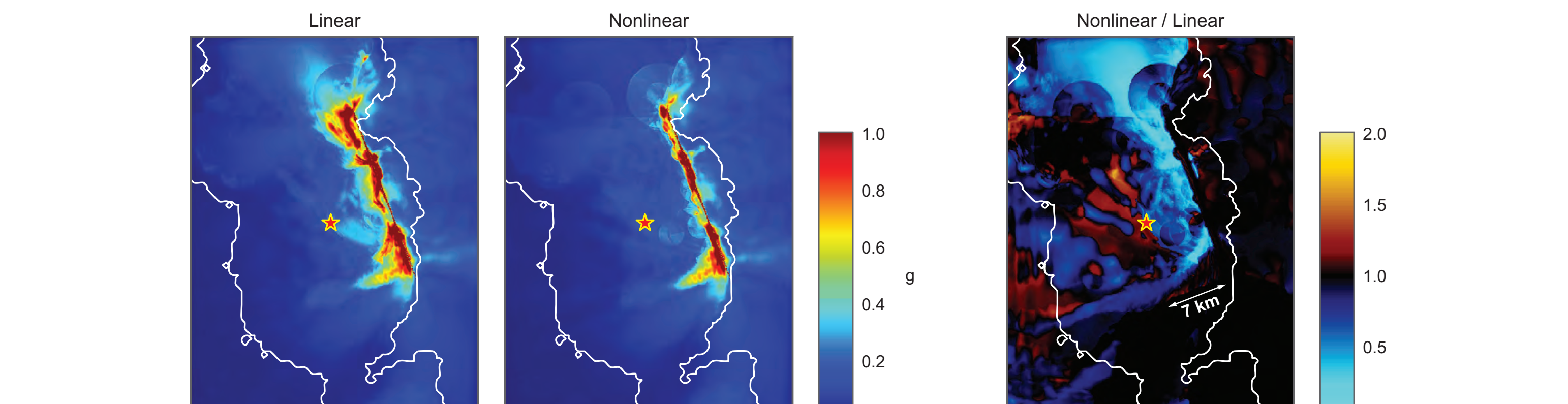


Figure 6: Comparison of the horizontal peak ground surface acceleration for the (a) linear and (b) nonlinear case, as a fraction of gravity; and (c) the ratio between the two cases (nonlinear over linear).

Figure 6 shows the comparison of the peak ground horizontal accelerations between the linear and nonlinear simulations. Maxima in both cases occur near the fault line and above the fault's plane projection on the surface. The color scale saturates at 1 g, with the linear simulation exhibiting larger areas with peak values greater than 1 g than the nonlinear case. The ratio of the two shows that in many areas the nonlinear case has lower values of peak acceleration than the linear case, though there are areas of amplification as well. The greatest differences are concentrated near the center and north of the fault.

Figure 7 shows the permanent displacement of both the linear and nonlinear simulations, computed as the average value of displacement over the last 15 seconds of simulation. The two cases present a similar pattern. Maximum permanent displacements are imposed by the slip prescribed at the fault with the largest values at the center near the surface and towards the bottom corners. Both simulations also preserve the same four regions of minima. The nonlinear simulation, however, presents a less homogeneous distribution of the maxima.

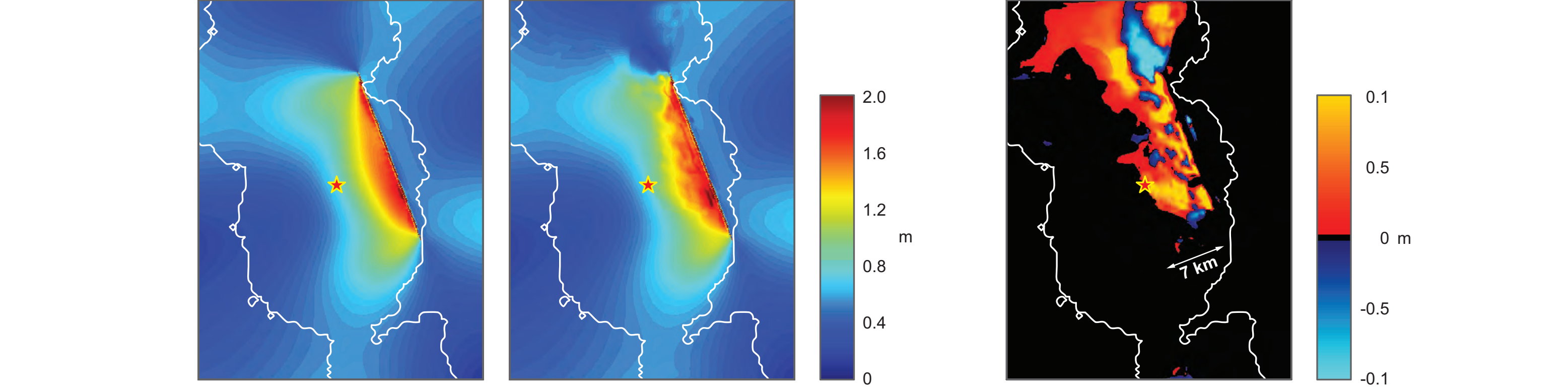


Figure 7: Magnitude of the surface permanent displacements. (a) Linear case, (b) nonlinear case, and (c) nonlinear - linear.

Local Response

Figure 8 shows the shear stress-strain relationships, for an array of points beneath station S11 (see Fig. 1 for reference). The V_s and V_p wave velocity profiles beneath the station are shown as reference, down to a depth of 210 m. The more pronounced plastic deformations occur at 175 and 210 m, where strains in the non-linear case reach values larger than twice the maximum linear strain. In general, shear components σ_{xy} and σ_{yz} are dominant over the horizontal σ_{xz} shear. This is an expected behavior due to the normal orientation of the fault's rupture. The coupling between the three components is clearly a 3D effect that cannot be captured with simplified 1D and 2D simulations.

Figure 9 shows the displacements in the two horizontal components of motion at five different stations throughout the region (see Fig. 1). In the *NS* direction, all stations present similar or larger values of permanent deformation in the nonlinear case than in the linear one. This may be interpreted as the result of a stronger directivity effect. For the case of station S6, contrary to common belief, the displacements in the nonlinear case are significantly smaller than in the linear case. This is possibly related to the proximity of this station to the east boundary of the basin. Furthermore, it indicates the presence of stronger basin effects.

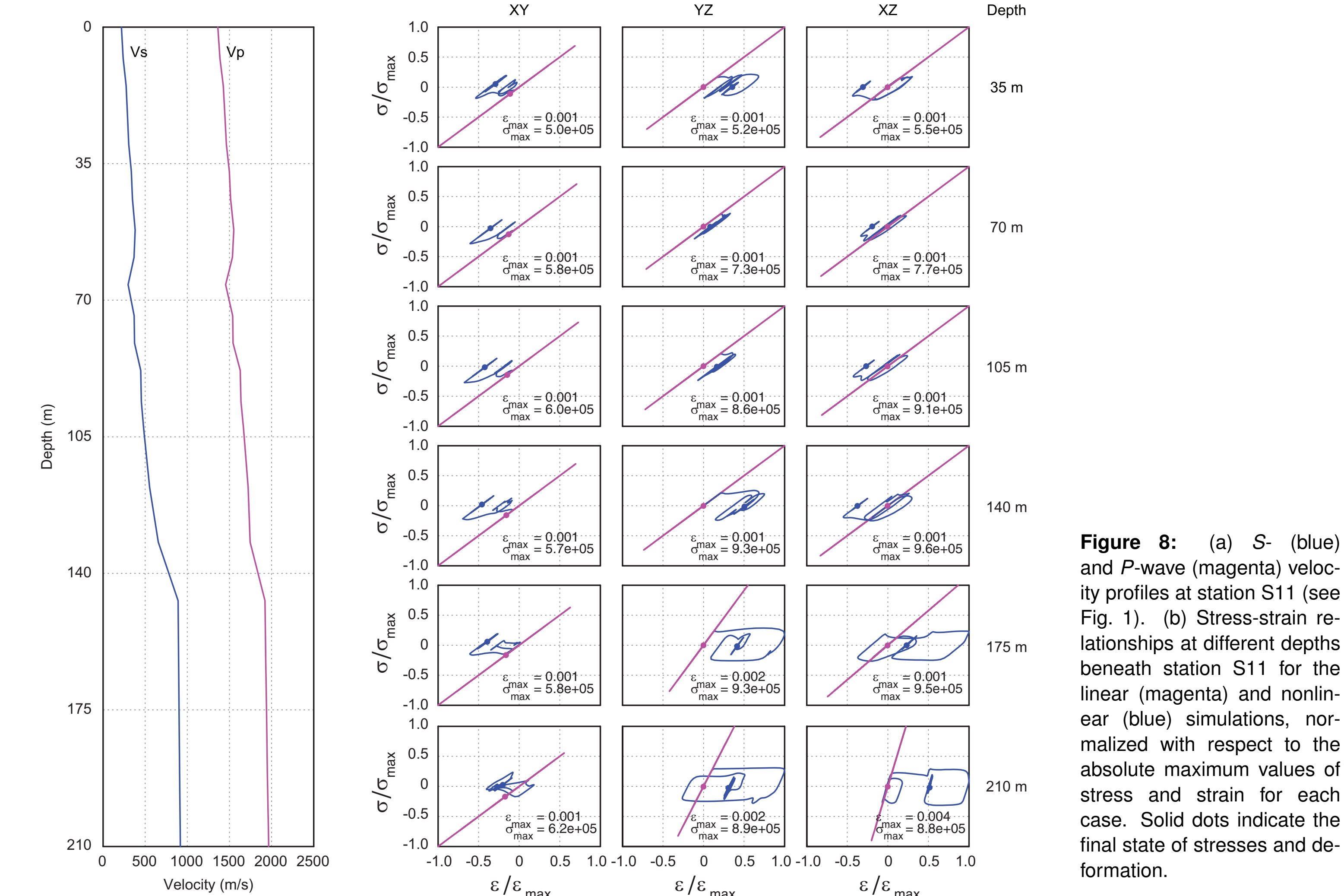


Figure 8: (a) S- (blue) and P-wave (magenta) velocity profiles at station S11 (see Fig. 1). (b) Stress-strain relationships at different depths beneath station S11 for the linear (magenta) and nonlinear (blue) simulations, normalized with respect to the absolute maximum values of stress and strain for each case. Solid dots indicate the final state of stresses and deformation.

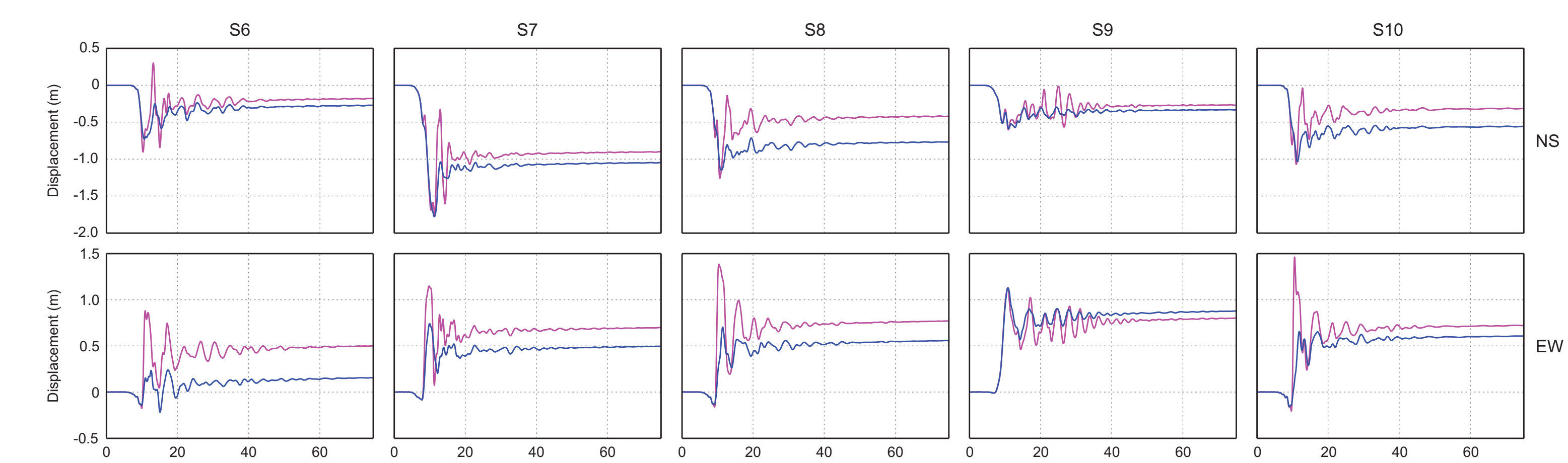


Figure 9: Comparison of the surface linear (magenta) and nonlinear (blue) displacement at stations S6, S7, S8, S9, S10 (see Fig. 1).

Figure 10 shows a comparison of the synthetics for ground accelerations at five different stations in both the time and frequency domains. By contrast, stations S3 and S4 do not show any significant influence of non-linearity. The comparisons in the frequency domain consistently show reductions of about 50 percent or more in the amplitude of the non-linear response with respect to the linear results.

In S1 and S5 the reductions are of the same order in both components of motion. For station S2, the reductions are predominant in the *NS* direction, whereas

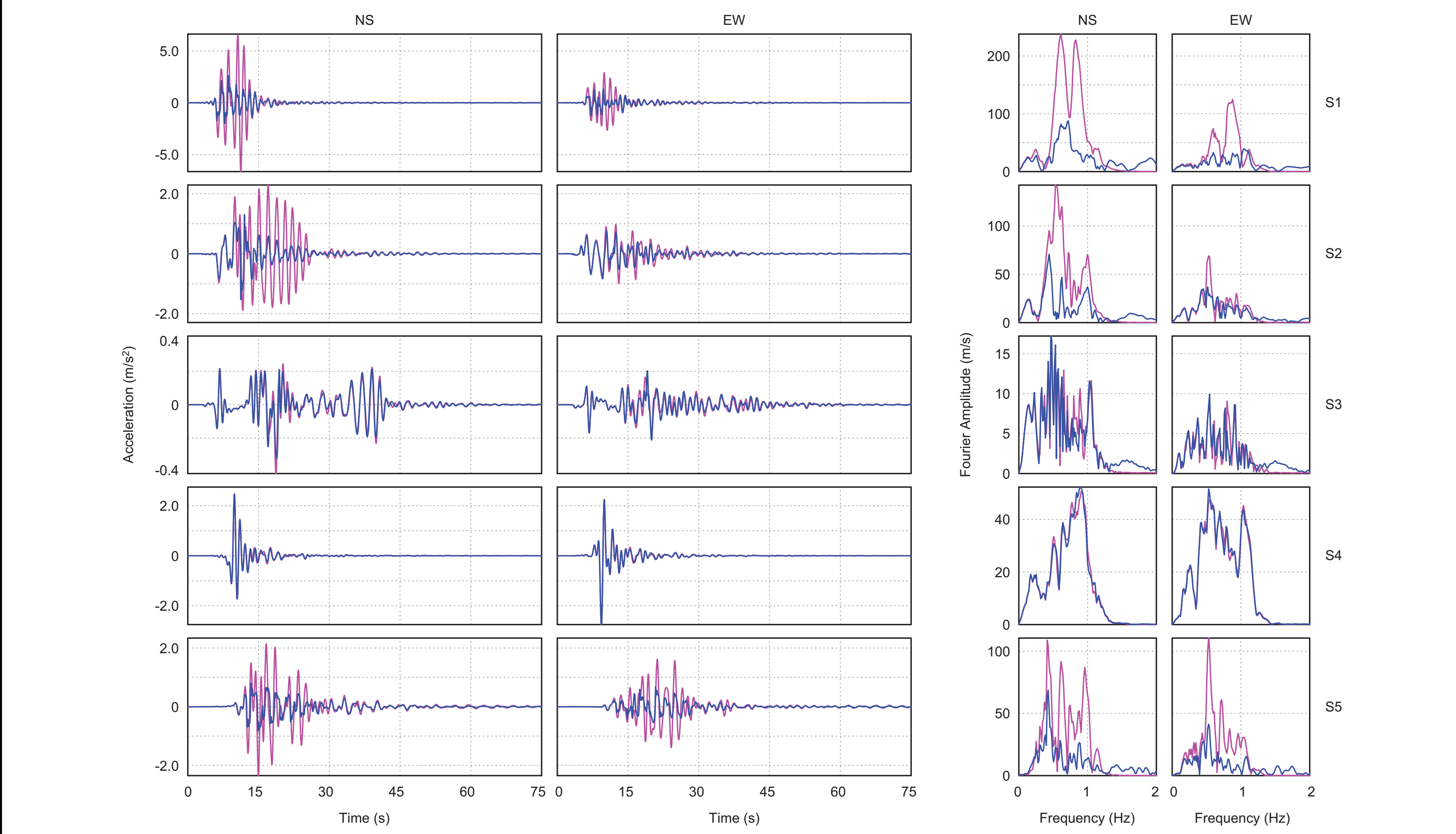


Figure 10: Comparison of the surface linear (magenta) and nonlinear (blue) accelerations (left) and their corresponding Fourier's amplitude spectra (right) in the *NS* and *EW* components of motion at stations S1, S2, S3, S4, S5 (see Fig. 1).

Implications for Engineering Design

Figure 11 shows the spectral acceleration (S_a) values throughout the region as a fraction of g , obtained from response spectra ordinates for periods $T_c = 1.5$ and 2.0 s. These periods are representative of mid-rise buildings. Results for the linear simulation indicate that structures with natural periods in this range and within a distance of about 10 km from the fault line could be exposed to pseudo accelerations larger than 1 g. In the nonlinear case, however, $S_a(g)$ of this level are present only in the immediate vicinity of the fault line (≤ 2 km), in the central and northern areas. This implies that soil nonlinearity can significantly change the excitation levels—generally a reduction—for particular periods of interest. No changes are observed far from the source or outside the basin.

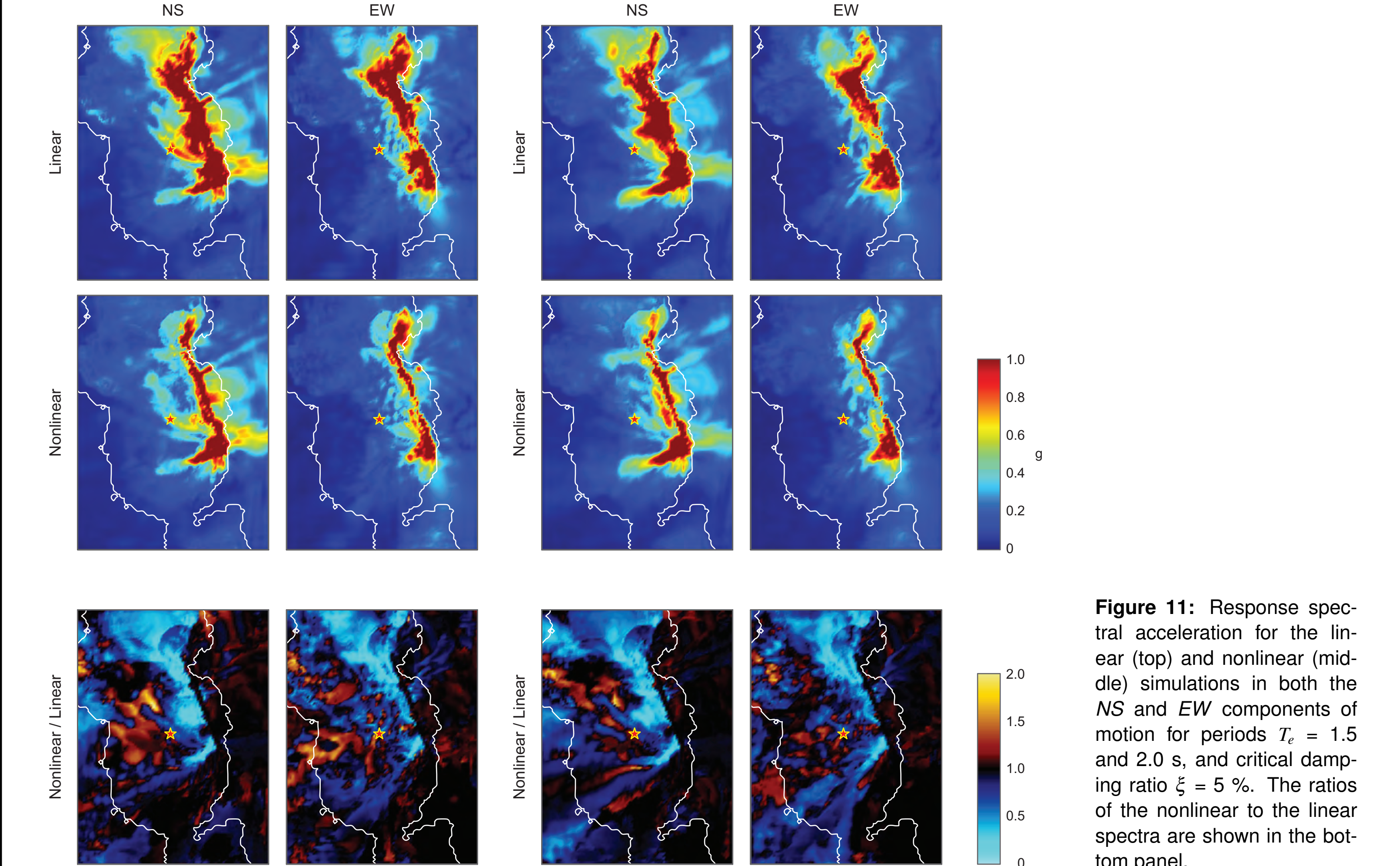


Figure 11: Response spectral acceleration for the linear (top) and nonlinear (middle) simulations in both the *NS* and *EW* components of motion for periods $T_c = 1.5$ and 2.0 s, and critical damping ratio $\xi = 5\%$. The ratios of the nonlinear to the linear spectra are shown in the bottom panel.

Concluding Remarks

We presented an application of a methodology for introducing the effects of nonlinear soil behavior in full 3D deterministic earthquake simulations at regional scales. Results from comparing the ground motion obtained for a M_w 6.8 scenario earthquake under linear anelastic and nonlinear elasto-viscoplastic material conditions in the soft-soil deposits in the Salt Lake City basin indicate that soil nonlinearities may cause significant changes in the distribution of permanent deformations, and reductions

in peak ground accelerations down to amplitudes of 20 to 50 percent of the peak response obtained under linear anelastic conditions. They underscore the importance that local site effects and soil nonlinearity may have on the ground response, and most importantly, the implications for structural engineering design and analysis. Additional work is still required to properly use and model more realistic properties and characteristics of the soil.

References

Liu, Q. and R. Archuleta (2011). Personal communication.
Magistrale, H., K. B. Olsen, and J. C. Pechmann (2006). Construction and verification of a Wasatch Front Community Velocity Model: Collaborative research with San Diego State University and the University of Utah. Final Technical Report 06HQGR0012. USGS, <http://earthquake.usgs.gov/research/external/reports/06HQGR0012.pdf>.
Perzyna, P. (1966). Fundamental problems in viscoplasticity. In Chernyi, G., Dryden, H., Germain, P., Howarth, L., Olczak, W., Prager, W., Probst, R., and Ziegler, R., editors, *Advances in Applied Mechanics*, Vol. 9, pp. 243-377. Elsevier.
Taborda, R. (2010). Three Dimensional Nonlinear Soil and Site-City Effects in Urban Regions. Ph.D. Thesis, Civil and Environmental Engineering, Carnegie Institute of Technology, Carnegie Mellon University, Pittsburgh, PA.